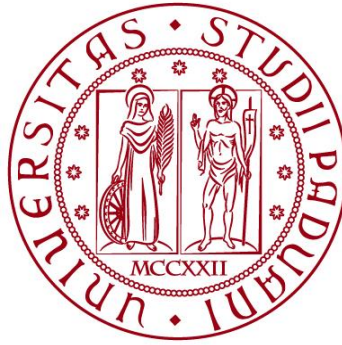# UNIVERSITÀ DEGLI STUDI DI PADOVA

DIPARTIMENTO DI BIOLOGIA

Corso di Laurea magistrale in Marine Biology

TESI DI LAUREA

Bisphenol A affects the antioxidant system of the Antarctic fish *Trematomus bernacchii*

Relatore: Prof. Gianfranco Santovito
Dipartimento di Biologia

Correlatore: Dott.ssa Elisabetta Piva
Dipartimento di Biologia

Laureando: Fabio Baroni

ANNO ACCADEMICO 2024/2025

CONTENTS

Abstract:

In recent decades, the amount of pollutants reaching the Antarctic region has exponentially increased, making it essential to understand how the native biota respond to them. The study aims to detect differences in responses of the antioxidant system of *Trematomus bernacchii* when exposed to bisphenol A (BPA) compared to the control conditions. The organs of interest are the brain and liver. Different biochemical assays were performed to determine the activity of: CAT (catalase), SODs (Superoxide dismutases) and Se-GPXs (Selenium-dependent Glutathione peroxidases). On average, the exposed group showed reduced activity compared to the control group. In the liver, CAT was decreased significantly in terms of activity. In the brain, SOD and GPX showed an even greater reduction of activity in the treated group compared to the control. This suggests an effect of BPA on the performance of the antioxidant system. Results were also supported by molecular analysis, such as qPCR. The gene CAT was downregulated in the liver, while the genes for SOD and GPX were downregulated in the brain. This could be an indication of BPA's capability in going through the blood-brain barrier or a response mechanism to save energy due to the stress of the exposure.

1.Introduction

1.1 Geographical information and general features

The Antarctic continent is in the southernmost part of the planet, surrounded by the Southern Ocean, geographically and climatically isolated from the other continents due to the presence of the Antarctic Circumpolar Current (ACC), one of the strongest marine currents in the world (Clarke et al., 2005).

The continent covers an area of approximately 13,375,000 km² and contains about 90% of the world's total ice and snow. It also has the highest average elevation compared to any continent; in fact, 55% of its area lies above 2000 meters. The western part of Antarctica is characterised as an archipelago of islands, while the eastern part shows a considerable amount of bedrock highly above the sea level (Dalrymple, 2013).

The climatic conditions are extreme, with the lowest temperature ever recorded on earth -89.2°C (Turner et al., 2009). Depending on the location considered, the average temperature may range from -10°C to -55°C. Due to these peculiarities, Antarctica has a significant influence on the global climate. The Antarctic continent also contains approximately 62% of the freshwater reserve. (Timmermann et al., 2001).

This once-pristine ecosystem is suffering from global change scenarios and anthropogenic activities. In particular, the highest melt rates are observed near the ice fronts and in deeper sub-ice cavities and compartments (Jacobs et al., 1992).
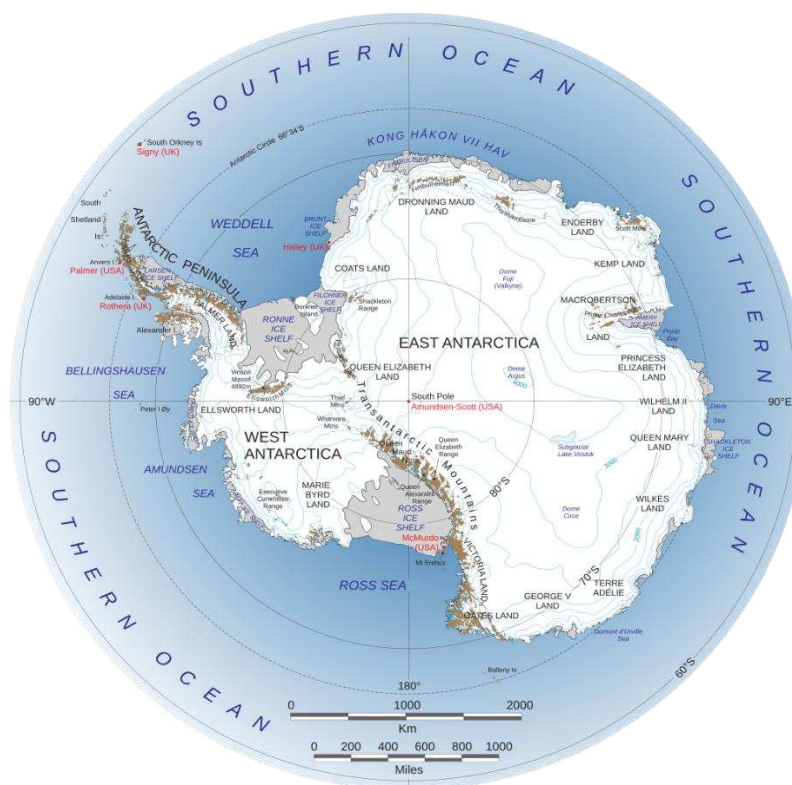

Figure 1: Map of Antarctica

Over centuries, local flora and fauna have evolved unique adaptations to survive in this region, resisting temperatures below zero and also surviving on local resources (Chown et al., 2015).

1.2 Antarctic Marine Environment

The Southern Ocean that surrounds the continent is a biodiversity hotspot due to its unique characteristics, including currents, temperatures, and fluctuations in ice quantity. The species listed are more than 8,200 (Griffiths, 2010).

One of the most interesting adaptations is related to Antarctic icefish. Over the centuries, they lost the capacity to produce haemoglobin. This characteristic is compatible with life only in this region, and low temperatures are essential for this functionality.

The region is also characterised by nutrient upwelling due to biological nutrient production. Local microorganism communities are responsible for this production and the cycle of these elements (Holm-Hansen, 1985). These processes are essential for the growth and proliferation of phytoplankton, which is at the base of the food web even here.

However, due to recent changes and shifts in local communities, there is also increasing concern related to the possibility of invasive alien species settling in this ecosystem and changing it forever. Human activity and human-induced changes are playing a key role in this kind of relationship between different ecosystems and possible invasions (McCarthy et al., 2019).

1.3 Antarctic Fish

Antarctic fish, particularly those belonging to the suborder Notothenioid, have developed a range of physiological and biochemical adaptations that enable them to survive in the extreme conditions of the Southern Ocean. One of the most remarkable examples is the production of antifreeze glycoproteins, molecules that prevent body fluids from freezing even at very low temperatures (Chen et al., 1997).

Another peculiar adaptation is the low haemoglobin concentration in blood, which optimises oxygen transport and blood fluidity in cold waters, where oxygen solubility is high and metabolic rates are reduced (Bargelloni et al., 1998).

The antioxidant enzymes and the whole antioxidant system of Antarctic fish, such as *Trematomus bernacchii*, have been optimised to work at low temperatures and high oxygen concentrations, conditions which may increase the risk of ROS production. This species possesses increased levels of glutathione and glutathione reductase compared to other species present in the area of Baia Terra Nova (Benedetti et al., 2010).

1.4 Fish Liver

The organisation of the hepatic tissue in the liver may vary according to the physiological characteristics of the species analysed, as well as its diet and reproductive status (Franco-Belussi et al., 2012).

Rich in lipids, the liver is the most critical organ used for detoxification, so it's essential to study how it is affected to identify the possible sensitivity of the fish to certain chemicals such as BPA. Being so rich in fats, it is likely that an accumulation of substances can be found here. Due to that, this organ may also be used as a bioindicator to detect the presence of possible toxic substances in the environment early. Moreover, an alteration in this organ may have an impact on the organism's ability to remove toxic xenobiotics (Kime, 1998).

In fish, the liver is a key organ for studying the effects of pollutants, toxins, parasites, and microorganisms, as these factors can alter its structure and, consequently, affect metabolic processes. Owing to its central role in metabolism and other physiological functions, the liver is also widely used as a proxy for assessing fish health status (Giltrap et al., 2017).

1.5 Fish Brain

Anatomically, we can identify a central nervous system (CNS) and an autonomic nervous system (ANS) in fish. The brain, spinal cord, spinal nerves and cranial nerves characterise the CNS. The organisation of the fish brain is like that of other vertebrates. In particular, in fish, the ventral area of the brain is the most conservative structure from a phylogenetic point of view (Kristiansen et al., 2020).

The brain is one of the most active organs from a metabolic perspective. This organ has a peculiar characteristic, which is the blood-brain barrier, a selective, semipermeable barrier that protects the brain from harmful substances while allowing essential nutrients to pass through. Due to its presence, the brain is isolated from the systemic circulation (Soengas and Aldegunde, 2002).

Neurotoxicity can also alter the behaviour of the fish. Resulting in strange swimming patterns and listlessness, isolation and alteration of feeding activity (Puga et al., 2016).

1.6 Pollution in Antarctica

Across the centuries, the human presence in the Antarctic region has increased. At the beginning of the 20th century, humans started to exploit the area with hunting, fishing and exploration activities. Due to these kinds of activities, the number of invasive species also increased on many sub-Antarctic islands. While more recently, fuel combustion, to move in the region, accidental oil spills, waste incineration and sewage have led to a further increase of xenobiotics. Moreover, the grasshopper effect is a natural phenomenon responsible for the arrival of a wide range of toxic substances. The contaminants are also capable of accumulating in the tissues and organs of local fauna and flora (Bargagli, 2008).

Traces of Persistent Organic Pollutants (POPs) are present in the snow of the region. To date, there are many knowledge gaps related to the presence of the substances on the continent (Vecchiato et al., 2015).

These substances pose a threat to local biota. Because prolonged exposure to anthropogenic pollutants—both legacy and emerging contaminants—as well as

pathogenic microorganisms in the vicinity of coastal research stations, may exert additive or even synergistic impacts on marine organisms. Many Antarctic marine species are endemic and possess unique ecophysiological traits, which, combined with the additional pressure of climate-related stressors, may increase their vulnerability (Bargagli and Rota, 2024).

1.7 Bisphenol-A (BPA)

Bisphenol A (BPA) is an artificial organic compound widely employed around the world in the manufacturing of polycarbonate plastics and epoxy resins used as a monomer. Due to the increasing global demand for plastic, the production of this compound has also increased through the years. This also explains why it's persistent in the waters even if it's susceptible to degradation. It acts as an endocrine disruptor by mimicking estradiol, binding to and activating the same estrogen receptors as the natural hormone. One peculiar characteristic is that it is capable of persisting more in seawater compared to freshwater in the absence of degradation (Biswal et al., 2020).

This substance can enter and contaminate seawater through multiple pathways, including the degradation of plastics and microplastics already present in the marine environment (Liu et al., 2019). Additional sources include wastewater effluents, accidental spills, and industrial discharges.
These chemicals can reach the Antarctic continent through long-range atmospheric transport (LRAT). Once they arrive, they start to accumulate in living organisms and build up in sediments (Han et al., 2016).

1.8 Oxidative Stress and Reactive Oxygen Species (ROS)

Organisms such as fish must maintain homeostasis, a condition in which the internal conditions of the animal are maintained constant. This means that when stress occurs, the potential uncontrolled production of reactive oxygen species resulting from it must be kept under control. One of the most critical and complex systems that can restore homeostasis in living organisms is represented by the antioxidant system. *ROS* are highly reactive molecules (or free radicals) derived from oxygen. They are generated during aerobic metabolism during the oxidative phosphorylation aimed at the synthesis of ATP following a reaction with electrons. They can cause oxidative damage to biomolecules if not properly balanced (Sies et al., 2017).

In fact, the vast majority of ROS are produced inside mitochondria, and approximately 4–5% of oxygen in the human body is converted to ROS by biological reductants (Jomova et al., 2023).

When the organism is under stressful conditions, the production of ROS increases. Among those conditions, there is also exposure to contaminants such as BPA, as well as rising temperatures. Inflammatory state also favours their production because immune system cells such as neutrophils and macrophages can produce ROS as a defence mechanism against pathogens (Chowdhury and Saikia, 2020).

ROS must not be considered harmful at all; in fact, they are needed for many essential signalling reactions. Not only that, but they are also helpful for cellular

proliferation and differentiation, as well as adaptations. The problems appear when they are produced in excessive numbers, and the organism cannot mitigate this condition. At physiological levels, they are considered good, while oxidative stress is the breakdown of the balance between the production and the elimination of ROS (Mittler, 2017).

Reactive oxygen species (ROS) can interact directly with nucleic acids, leading to oxidative modifications and mutations that may contribute to the initiation and progression of various pathologies, including carcinogenesis. Moreover, ROS can target polyunsaturated fatty acids within cellular membranes, initiating lipid peroxidation, a self-propagating chain reaction that compromises membrane integrity and fluidity, potentially culminating in cellular apoptosis or necrosis. Elevated ROS levels can also impair mitochondrial function by damaging mitochondrial DNA and disrupting the electron transport chain, thereby exacerbating oxidative stress and bioenergetic failure (Jomova et al., 2023).

1.8.1 SUPEROXIDE ANION ($\bullet O_2^-$)
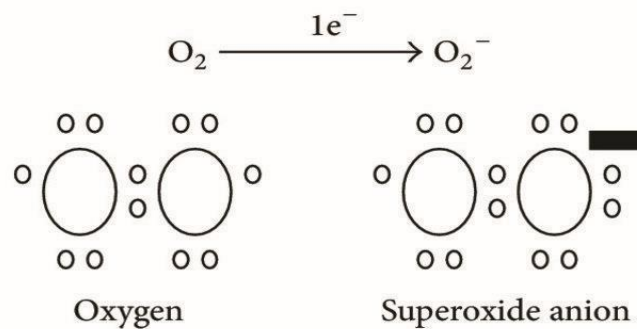
Figure 2. Superoxide anion formation.

The superoxide anion $\bullet O_2^-$, is considered the primary ROS since it is the first intermediate formed in the electron transport chain (ETC) (Valko et al., 2004). Among all the ROS, it is the one that exhibits a relatively low reactivity in interactions with biological molecules, and usually reacts with reduced molecules (Jomova et al., 2023). Nicotinamide adenine dinucleotide phosphate reduced (NADPH) is the coenzyme that mitigates this anion.

1.8.2 HYDROGEN PEROXIDE (H2O2)
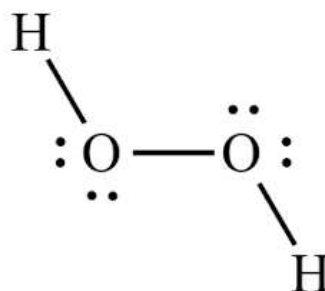
Figure 3. Hydrogen peroxide Lewis's structure

Hydrogen peroxide (H_2O_2) is derived from the dielectronic reduction of molecular oxygen, and it is considered the least dangerous among ROS. It is usually

produced inside peroxisomes when hydrogen enters the organelle through pumps. It can also be formed under inflammatory conditions due to pathogens (Jomova et al., 2023).

1.8.3 HYDROXYL RADICAL (•OH)
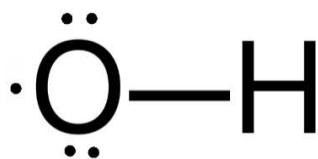
Figure 4. Hydroxyl radical Lewis's structure

This ROS derives from the trielectronic reduction of molecular oxygen, since it is the most reactive among all ROS, it's also considered the most dangerous. In addition to this, there is no enzyme capable of eliminating this molecule; hence, the best way to mitigate the damage is to reduce its production. There are two reactions responsible for its formation, so reducing its precursors is also a way of prevention.
Haber-Weiss reaction

$$\bullet O_2^- + H_2O_2 \rightarrow \bullet OH + OH^- + O_2$$

and the Fenton reaction

$$Fe^{2+} + H_2O_2 \rightarrow Fe^{3+} + \bullet OH + OH^-$$

1.8.4 SINGLET OXYGEN ($*O_2$)
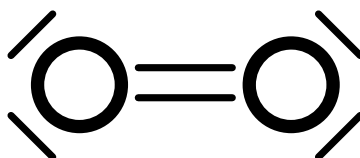
Figure 5. Lewis's structure of singlet oxygen

Singlet oxygen, similarly to hydrogen peroxide, lacks unpaired electrons in its outer electron shell and is classified as a reactive diamagnetic molecule. It is the least excited state of molecular oxygen. (Jomova et al., 2023).

1.8.5 PEROXYLIC RADICAL (ROO•)
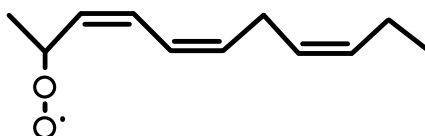
Figure 6. Peroxyl radical structure

The peroxyl radical (ROO•) is a reactive oxygen species formed primarily through the reaction between alkyl radicals (R•) and molecular oxygen (O_2). It plays a central role in oxidative chain reactions, particularly in lipid peroxidation, where it propagates membrane damage by abstracting hydrogen atoms from adjacent

polyunsaturated fatty acids. Phospholipid, once oxidised, does not return to a normal state because the modification is not reversible. This process contributes significantly to cellular dysfunction under conditions of oxidative stress.

1.9 Antioxidant system

The antioxidant system is a complex network of enzymatic and non-enzymatic components that work synergistically to neutralise reactive oxygen species (ROS) and protect cells from oxidative damage. A system that is essential in evolution, especially in areas of increasing pollutant concentration that cause increasing stress to species.

Fish that possess different ecological needs may exhibit diverse responses to environmental pollutants. Assessing antioxidant system performance is essential in environmental studies (Atli et al., 2016).

1.10   Non-enzymatic antioxidant responses

Non-enzymatic antioxidant defences consist of a variety of low molecular weight compounds capable of directly neutralising reactive oxygen species (ROS). These molecules act not only as free radical scavengers but also as regenerators of other antioxidants, contributing to the maintenance of cellular redox homeostasis. Key non-enzymatic antioxidants include glutathione (GSH), vitamin E (α-tocopherol), vitamin C (ascorbic acid), carotenoids (such as astaxanthin), polyphenolic compounds and metallothioneins (MT). Their synergistic action enhances the cellular capacity to counteract oxidative insults, especially under conditions of environmental or metabolic stress (Abouelenein et al., 2022).

1.11   Enzymatic antioxidant response

Antioxidant enzymes are proteins whose primary function is to convert reactive oxygen species (ROS) and their derivatives into more stable and typically less harmful compounds. They play a key role in protecting cells from oxidative stress caused by ROS accumulation. Some of them work synergistically to face stress conditions (Jomova et al., 2023).
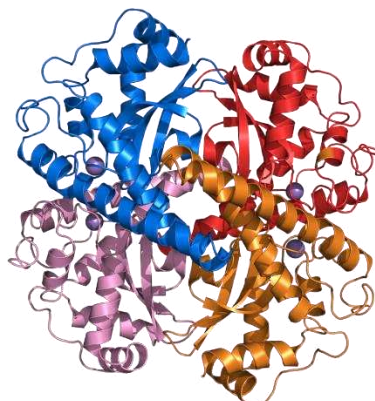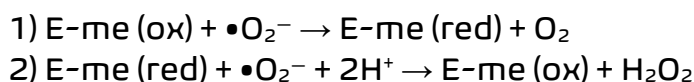
1.11.1   Superoxide dismutase (SOD)

Figure 7. Crystal structure of the antioxidant enzyme SOD isoform 2 (Mn-SOD)

SOD, primarily found in the cytoplasm, is regarded as one of the most efficient antioxidant enzymes. It catalyses the dismutation of the superoxide anion radical with high effectiveness. In humans, there are three different isoforms: Cu, Zn-SOD (SOD1), Mn-SOD (SOD2), and EC-SOD (SOD3) (Jomova et al., 2023).

SOD1 is in the cytoplasm of cells (also the most common in animals), while SOD2 is mainly localised in mitochondria and SOD3 in the lungs.

There are two reactions in the process for dismantling ROS:

1) $E\text{-me (ox)} + \bullet O_2^- \rightarrow E\text{-me (red)} + O_2$
2) $E\text{-me (red)} + \bullet O_2^- + 2H^+ \rightarrow E\text{-me (ox)} + H_2O_2$

At the end, we have that one SOD eliminates two molecules of $\bullet O_2^-$, producing oxygen and H_2O_2. SOD can be considered the most powerful among antioxidants (Ighodaro and Akinloye, 2018).

1.11.2 GLUTATHIONE PEROXIDASE (GPx)

The glutathione peroxidase (GPX) family comprises eight known members (GPX1–GPX8) and is recognised for its diverse functions that influence nearly all cellular processes. These enzymes have long been associated with antioxidant defence, playing a crucial role in mitigating oxidative stress and preserving redox homeostasis. However, each GPX isoform differs in its mechanism of action and cellular localisation, contributing uniquely to the regulation of redox balance (Pei et al., 2023).

In most cases, GPX activity relies on a micronutrient cofactor, which is selenium. Due to this dependence, GPX is commonly referred to as a selenocysteine-containing peroxidase.

GPx1 is the most abundant selenoperoxidase and is expressed in virtually all cell types. It is primarily located in the cytoplasm and mitochondria, where it catalyses the reduction of hydrogen peroxide and organic hydroperoxides using glutathione (GSH) as a substrate, thereby protecting cells from oxidative damage.

GPx2 is predominantly expressed in the gastrointestinal tract, especially within the intestinal epithelium. Its function is closely related to the maintenance of mucosal redox balance and the detoxification of ingested hydroperoxides. Like GPx1, it is a selenocysteine-containing homotetramer.

GPx3 is mainly found in the kidneys but is also present in extracellular fluids, including plasma, as a secreted glycoprotein. It serves as an essential systemic antioxidant, scavenging circulating peroxides and maintaining extracellular redox balance.

GPx4 is unique within the GPx family due to its monomeric structure and its substrate specificity. It is the only isoform capable of reducing complex phospholipid hydroperoxides directly within cellular membranes. GPx4 is expressed in multiple cellular compartments—including the cytosol, mitochondria, and nucleus—and exists in different isoforms depending on localisation. It also plays a critical role in preventing ferroptosis and in sperm

development, where it fulfils structural functions independently of its peroxidase activity.

GPx5 is expressed exclusively in the epididymis of male mammals and is secreted into the lumen to protect maturing sperm from oxidative stress. Unlike other GPx enzymes, GPx5 does not contain selenocysteine and is therefore classified as selenium independent.

GPx6 is expressed in the olfactory epithelium and, in humans, exists as a selenoprotein, whereas in rodents it contains cysteine instead of selenocysteine. Although its precise function is not yet fully understood, it is believed to be involved in detoxification processes related to olfactory signalling.

GPx7 is localised within the lumen of the endoplasmic reticulum (ER). Unlike classical GPx enzymes, it lacks peroxidase activity in the traditional sense and does not contain selenocysteine. Instead, it acts as a redox sensor and transducer, promoting disulfide bond formation during protein folding by transferring oxidative equivalents to protein disulfide isomerases (PDIs).

GPx8 is another ER-resident protein, anchored to the ER membrane. Like GPx7, it lacks selenocysteine and does not use GSH as a reducing agent. Its primary role involves regulating hydrogen peroxide flux between the ER and other cellular compartments and assisting in oxidative protein folding through its interactions with Ero1α and PDI.

Together, the GPx isoforms form a highly specialised antioxidant network that protects cells from oxidative damage, supports redox homeostasis, and contributes to various physiological processes across different tissues and cellular compartments. (Ighodaro and Akinloye, 2018).

GPXs catalyse the reduction of hydrogen peroxide or organic hydroperoxides into water or their corresponding hydroxyl compounds through a divalent reduction, using reduced glutathione (GSH) as the electron donor.

$$2GSH + H_2O_2 \rightarrow GSSG + 2H_2O$$
$$2GSH + R\text{-}OOH \rightarrow GSSG + R\text{-}OH$$
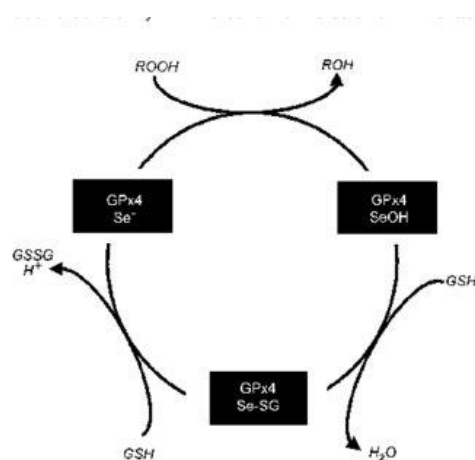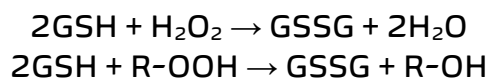
Figure 8. Reaction of Se-GPx against ROS

1.11.3   Catalase (CAT)
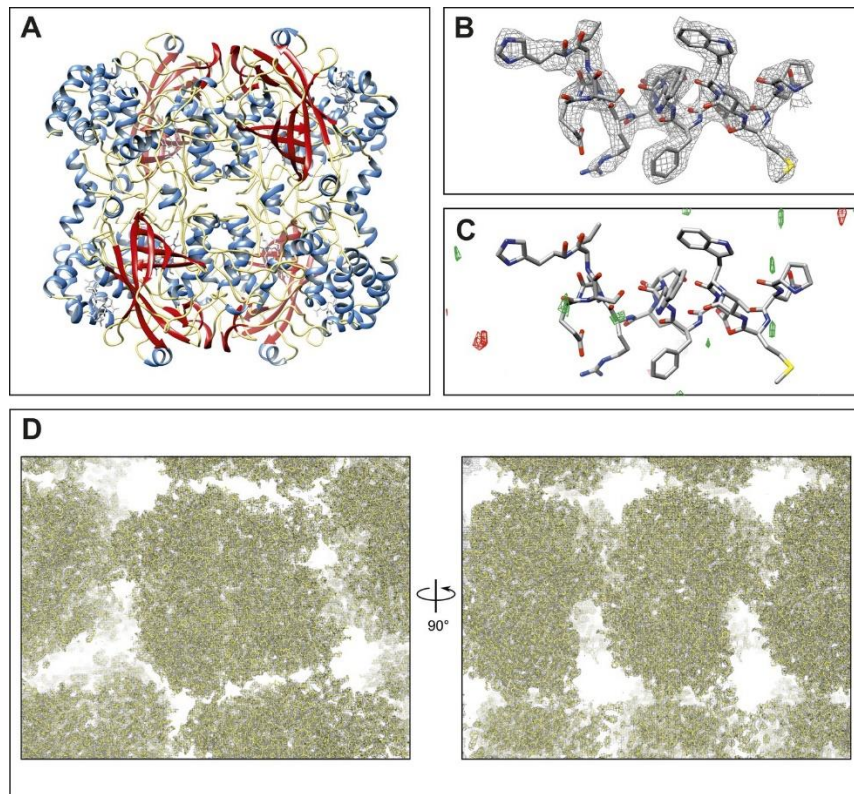
Figure 9. Structure of catalase determined by using MicroED. Picture from (Nannenga et al., 2014).

Catalase is a ubiquitous enzyme found in nearly all living organisms, including bacteria, fungi, plants, and animals, and is primarily located in peroxisomes. It decomposes hydrogen peroxide (H_2O_2) into water and oxygen, serving as a vital defence mechanism against oxidative stress (Deisseroth and Dounce, 1970).

Catalase is composed of four identical subunits, as shown in Figure 9. It is primarily localised in subcellular compartments, especially within peroxisomes, where it facilitates the decomposition of hydrogen peroxide into water and molecular oxygen. This is considered auxiliary to GPx.

$$2H_2O_2 \rightarrow O_2 + 2H_2O$$
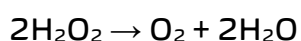
The catalytic process occurs in two sequential steps. Initially, one molecule of H_2O_2 is converted into water, resulting in the formation of an oxoferryl intermediate. In the second step, the enzyme returns to its reduced state through a reaction with a second H_2O_2 molecule (Alfonso-Prieto et al., 2009).

1.11.4   PEROXIREDOXINS (Prdx)
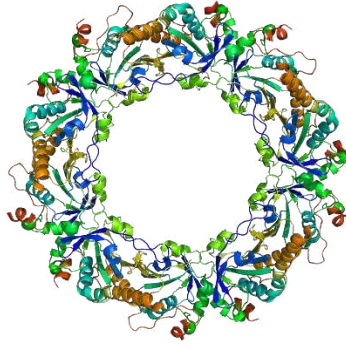
Figure 10. Crystal structure of *PRDX4*

PRDXs are a multigene family of peroxidase-active enzymes ubiquitously present across living organisms, very large and highly conserved. The peroxidase activity of Prdx enzymes toward H_2O_2, organic hydroperoxides, and peroxynitrite plays a vital role in safeguarding cellular components from oxidative damage. However, the presence of multiple peroxide-scavenging enzymes such as catalase, GPx, Prx, and ascorbate peroxidase (APx) within the same organism, cell, or even subcellular compartment suggests that their functions extend beyond mere protection against oxidative stress (Rhee, 2016).

They catalyse the reduction of both organic and inorganic peroxides plus their hydroxyl derivatives, converting them to water.

$$2\text{Cys-SH} + \text{ROOH} \rightarrow \text{Cys-S-S-Cys} + H_2O + \text{ROH}$$

At present, six Prdx isoforms are known, belonging to three classes according to not only structure but also mechanism of action:

> ➤ Typical two-cysteine Prdxs (Prdx1, Prdx2, Prdx3, Prdx4);
> ➤ Atypical two-cysteine Prdxs (Prdx5);
> ➤ One-cysteine Prdxs (Prdx-6).

In the reaction, there are two different steps, centred around a redox-active cysteine residue known as the peroxidatic cysteine. All three Prdx classes in the initial phase act the same way: the peroxidatic cysteine attacks the peroxide substrate, resulting in its oxidation to sulfenic acid (Cys-SOH).

The second step, which regenerates the reduced cysteine, differs across the three classes:

Typical 2-Cys Prdxs function as homodimers and possess two conserved cysteine residues per subunit. Following sulfenic acid formation, Cys-SOH forms an inter-subunit disulfide bond with the resolving cysteine (Cys-SH) from the opposite subunit. While Atypical 2-Cys Prdxs, although also homodimeric, undergo intramolecular disulfide bond formation. Differently in this reaction, Cys-SOH reacts with a resolving cysteine within the same polypeptide chain. The third class 1-Cys Prdxs lack a resolving cysteine and, as such, the oxidised Cys-SOH is reduced back to its thiol form by external electron donors, such as thioredoxin or other low-molecular-weight thiols.

Prdx1 and Prdx2 are typical 2-Cys peroxiredoxins predominantly located in the cytosol and nucleus. They are mainly involved in neutralising hydrogen peroxide and regulating redox-sensitive signalling pathways that influence processes like cell growth and apoptosis.

Prdx3 is another typical 2-Cys peroxiredoxin, but it is specifically localised in the mitochondria. Its primary role is to detoxify hydrogen peroxide generated during mitochondrial respiration, thereby protecting mitochondrial structures from oxidative damage.

Prdx4 is found in the endoplasmic reticulum and extracellular space. It contributes to oxidative protein folding and participates in peroxide detoxification in secretory pathways.

Prdx5 belongs to the atypical 2-Cys subgroup and is distributed across several compartments, including the cytosol, mitochondria, peroxisomes, and nucleus. It can reduce a wide range of peroxides, reflecting its multifunctional antioxidant role.

Prdx6 is the only 1-Cys peroxiredoxin in mammals. It is primarily cytosolic but also found in lysosomes and lung lamellar bodies. Uniquely, it has both glutathione peroxidase and phospholipase A_2 activity, allowing it not only to reduce phospholipid hydroperoxides but also to participate in membrane repair and the regulation of oxidative burst responses (Lien et al., 2012; Rhee, 2016).

2.Aim of the study

The Antarctic region is characterised by an increase in the presence of various pollutants of anthropogenic origin. Therefore, there is growing concern about the potential impact of these chemicals on this ecosystem. BPA levels are rising worldwide, mainly due to the increasing amount of plastic produced by industries every year.

This project aims to investigate the potential toxic effects of BPA by examining differences in the antioxidant system responses between adult specimens of *Trematomus bernacchii* (*Boulenger*, 1902) exposed to 25 µg/L of BPA and unexposed controls.

Specifically, this thesis focuses on analysing the expression patterns of key genes and proteins involved in the antioxidant defence system, to investigate how different organs and cellular organelles react to BPA-induced toxicity. To achieve this aim, the brain and liver were chosen as crucial organs. According to the literature, they appear to be the most impacted organs by BPA-induced toxicity. The brain was chosen as the organ of interest because it appears that BPA is one of the few compounds capable of crossing the blood-brain barrier, thereby accumulating in this organ. Therefore, investigating the brain could highlight toxic effects uncommon to other environmental contaminants. Liver, on the other hand, due to its lipid-rich cells, is the primary accumulator of xenobiotics and toxic substances, making it the best bioindicator for this type of study. The analysis is focused on the following genes: *cat*, *gpx1*, *gpx3*, *gpx4*, *sod1*, *sod2, prdx3, prdx4,* and *prdx5.*

Understanding the plasticity of *Trematomus bernacchii's* antioxidant system in response to this stressor could provide an indication of its ability to cope with current and future global change scenarios. It will also help in understanding the potential impacts on other marine species that live in the region. The outcome from this study may also be used by policymakers to change the current level of production of BPA globally and to mitigate future levels of emissions. The research also highlights the increasing level of anthropogenic activity in an area that was previously uncontaminated and may struggle to cope with the growing stress related to pollution, increasing temperatures, and human presence.

3. Materials and methods

3.1   Target species and sampling site

The target species of this project is *Trematomus bernacchii,* an endemic Antarctic fish belonging to the Nototheniidae family. This species lives in waters that have a depth range which varies from 0 to 700 m, and it has an essential ecological role, being both a predator and a prey, for key species in this ecosystem. Nototheniids present peculiar adaptations to this kind of environment, like antifreeze glycoprotein, preventing the body from freezing, and organs modified to work better in low-temperature conditions to optimise oxygen transport.

Only 20 individuals of this species were sampled for this study to comply with the strict ethical regulations of scientific research in Antarctica. Adult specimens of *T. bernacchii* (n=20, length = 23.76 ± 2.99 cm, weight = 211.92 ± 80.40 g) were collected at the end of October 2022 from the Ross Sea at Baia Terra Nova (74°42'S, 164°7'E) using hook and line with artificial baits at depths of 60-100 m. Upon capture, the fish were temporarily kept in buckets and transferred to the aquarium facility at the Italian research station Mario Zucchelli, where they were maintained in aerated tanks (100 L each), the system was isolated during the exposure to avoid accidental BPA spill in the environment. The seawater temperature was held at 0.01 ± 0.02 °C, ensuring optimal acclimation conditions for five days to facilitate recovery from sampling stress. The tanks were covered to simulate a low-light regime or even near-dark conditions, aligning with their natural conditions at these depths. This setup also served to reduce stress caused by the presence of operators, thereby maintaining a controlled and less intrusive environment for the fish. During this period, fish were not fed, and water quality and temperature were carefully monitored to ensure optimal recovery conditions. Ten individuals were randomly selected and assigned to control conditions, and the remaining 10 were exposed to 25μl/L of BPA.

At the end of the experiment, 10 days long, the fish were euthanised with an overdose of clove oil (dissolved in seawater). Afterwards, the brain and liver were excised from all fish, all specimens were measured in length and weight, and the liver and spleen were also weighed separately. Each organ was divided into two pieces: one stored in RNA later and the other frozen in liquid nitrogen and kept at -80°C until subsequent analysis.

Figure 11: Picture of the Antarctic fish *Trematomus Bernacchii*

3.2   RNA Extraction:

Total RNA was extracted from tissue with TRIzol™ Reagent (Invitrogen) according to the manufacturer's protocol for all samples and tissues. TRIzol™ Reagent is a monophasic solution of phenol and guanidine isothiocyanate, optimised for the efficient and simultaneous extraction of high-integrity total RNA, DNA, and proteins from a variety of biological specimens, including cells and tissues. It can facilitate the lysis of cells, denaturation of proteins, and inactivation of RNases and DNases, allowing for the extraction.

Quantities of tissue were weighed (mean weight of brain = 30mg; mean weight of liver = 52mg) and cleaned using PBS (Phosphate-Buffered Saline) twice since they were kept in RNA Later. After that, they were inserted into a sterile Eppendorf tube. The following scheme was followed to perform the extraction.

DAY1:

1) Homogenization
    - Add 1 mL of TRIzol for 100 mg of tissue (scaling reagent according to the weight measured)
    - Homogenization was performed by using TissueLyser and aluminium beads

2) Phase Separation
    - Incubation at room temperature for 5 mins
    - Add 200 μL of chloroform for every 1 mL of TRIzol used
    - Vortex for 15 seconds and incubate at room temperature for 3 minutes
    - Centrifuge at 4°C 13000 rcf x 15 mins

    Chloroform is capable of inducing phase separation and dissolving protein, lipids and other cellular components since it's not polar, but it's unable to dissolve RNA. Due to that, an aqueous supernatant containing RNA is formed and easily distinguishable from other layers containing other components.

3) RNA precipitation
    - Transfer the supernatant to another Eppendorf tube without disturbing the interphase
    - Precipitate the RNA by mixing it with cold isopropyl alcohol (not supplied). Use 500 μL of isopropyl alcohol for every 1 mL of TRIzol used.
    - Vortex
    - Incubate samples for 10 minutes at room temperature
    - Centrifuge at 13000 rcf for 30 min at 4°C
    -
4) RNA Wash
    - Remove the supernatant without touching the RNA pellet
    - Wash the pellet once with 75% ethanol (not supplied), adding at least 1 ml of ethanol for each 1 ml of TRIzol used
    - Vortex
    - Centrifuge at 7500 rcf for 5 mins at 4°C

Repeat this process an additional time when finished.

5) RNA Resuspension and Purification
   - Remove the supernatant without touching the pellet
   - Air-dry the pellet under the chemical hood until it's dried completely (~10min)
   - Dissolve in PCR-grade water by pipetting up and down. The volume of the water must be proportional to the dimension of the pellet. Write down the water used.

     Incubate at room temperature for two hours.

6) RNA Purification
   - Incubate in warm bath 40°C for Maximum 5 mins
   - Centrifuge 13000 rpm for 15 min at 4°C
   - If a precipitate appears, transfer the supernatant to a clean Eppendorf
   - Precipitate the supernatant with litiocloride (1/3 of the water volume used for the resuspension phase)
   - Keep in the fridge on ice at 4°C Overnight

This last step is used to remove carbohydrates, and it's essential when working with Antarctic Fish. By doing that, the RNA obtained will be even more pure since fish from this area are characterised by high glycoprotein presence (ex., antifreeze glycoproteins).

DAY2:

7) RNA wash and last incubations
   - Centrifuge at 4°C at 13000 rcf for 20 mins
   - Remove the supernatant without touching the pellet
   - Wash the pellet with cold ethanol 75%
   - Vortex
   - Centrifuge at 4°C at 13000 rcf for 20 mins

   Wash again with ethanol
   - Remove the supernatant and air dry the pellet under the chemical hood for 10 mins or until it's completely dry
   - Resuspend the pellet in H2O RNAsi FREE: Volume proportional to the dimension of the pellet (≈ 40 µL)

     Incubate at room temperature for 2 hours.

   - Incubate in a warm bath at 55°C for 10 minutes
   - Vortex

RNA Extraction
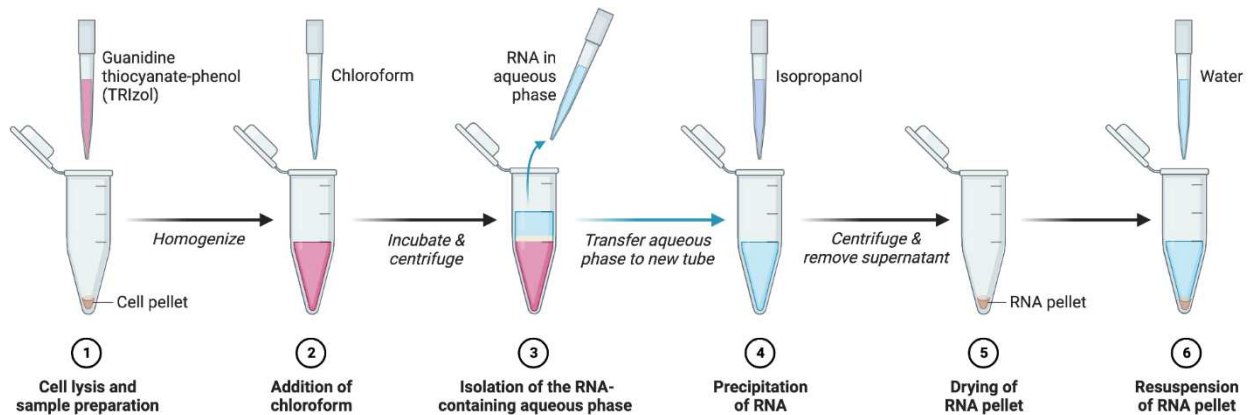
Figure 12: Schematic summary of RNA extraction procedure

3.3 RNA Quantification:

Once extracted, the RNA was quantified using a Spectrophotometer called Nanodrop, which measures the concentration of nucleic acids and proteins. The quantity necessary to obtain results is 1 µL of sample. The instruments perform readings at different wavelengths: 230, 260, and 280 nm to evaluate A260/280 and A260/230 ratios. For the A260/280 ratio, a result of ~2.0 is commonly accepted as "pure" for RNA. While A260/230 values should be in the range of 1.8-2.2, lower values might indicate possible contamination.

3.4 DNase Treatment:

After the extraction, the RNA can be contaminated with DNA in various amounts. Before proceeding with the treatments and analysis, it is essential to purify it. To do that, it is possible to follow a procedure which is performed in this case using the kit "*DNAse* Promega". The components were prepared according to the table 1.

Table 1: Contents for *DNase* Treatment

Components	Quantity
RNA	1 µl
DNAse	1 µl
RQ1 DNase 10X Reaction Buffer (M198A)	1 µl
PCR Grade Water	7 µl

After the preparation procedure in which everything listed is added to an Eppendorf tube of 0.5 ml, an incubation of 30 min at 37 °C in a thermocycler follows. It is during this incubation that the *DNase proceeds to degrade any residual DNA*.

After the incubation step, 1µl of *DNAse Stop Solution (EDTA)* is added to all samples, and an incubation of 10 min at 65 °C is needed to stop the activity of the enzyme to prevent further degradation that may have an impact on the *RNA* integrity. In the end, we will have a final volume of 11µl of RNA treated with DNase that can be used.

3.5 RNA Reverse transcription and cDNA synthesis:

The cDNA synthesis was performed using a Biotechrabbit™ cDNA Synthesis Kit, which is highly efficient in synthesising long cDNAs (≥19 kb). The kit contains RevertUP™ II Reverse Transcriptase that enables highly efficient reverse transcription with increased thermostability, an RNAse Inhibitor, which is a potent non-component inhibitor of RNases. Oligo (dT) primers were used for the synthesis of cDNA from only poly(A) tailed mRNA. Finally, Ribonuclease inhibitor is needed to prevent RNA degradation.

The *cDNA* synthesis reaction was performed with the reagents listed in Table 2.

Table 2: List of components for *cDNA* synthesis

Components	Volumes
dNTP Mix (10 mM each)	2
RNase Inhibitor, 40 U/µL	0.5
Oligo dT_{12-18} (10 µL)	0.5
5x Reserve Transcriptase Buffer	4
RNA Template	1
RevertUP^{TM} II Reverse Transcriptase	1
PCR Grade Water	Up to 20

Every test tube was then incubated in a PCR thermocycler at 50°-55° for 60 minutes and at 99°C for 5 minutes to inactivate the enzyme.
The product can last for several weeks if stored at -20°C.

3.6 Control PCR with housekeeping gene

To check if the obtained cDNA was still intact and without contamination, a PCR was performed. The primers used were already known and 100% working; they were primers of β-actin (housekeeping gene). On gel, these genes should produce only one band at 100-150 bp. Biotechrabbit™ provided the protocol followed. The primers before use were diluted 1:10. In the table below are listed the components to prepare our samples in different Eppendorf tubes (0,5 ml).

Table 3: List of components to do PCR according to protocol.

Components	Quantity
2X YourTaq PCR Master Mix	12,5 µl
Forward Primer	1 µl
Reverse Primer	1 µl
cDNA	2 µl
PCR Grade Water	8,5 µl

After a brief centrifugation, the samples were inserted into the thermocycler for incubation. Eppendorfs were incubated in the thermocycler set with the following parameters (Figure 13):

- Initial activation: 2 minutes at 95 °C (this favours complete denaturation of the cDNA).
- Annealing (35 cycles): 30 s at 95 °C (denaturation), 30 s at the chosen annealing temperature (annealing), 30 s at 72 °C (extension).
- Extension: 5 minutes at 72°C to ensure the amplicons have been fully amplified.

Optimising the annealing temperature is essential: if it's too low, non-specific amplification may occur, while if it's too high, amplification may fail altogether.

Figure 13: The thermocycler display shows time, temperature, and number of cycles for each PCR step.

Gel for electrophoresis was prepared using 2.4 g of agarose in 120 mL of TAE 1X. The quantity of agarose and TAE was the best suggested for the 50bp DNA ladder used. The dye was added according to the following proportion:

Dye : Sample = 1 : 5

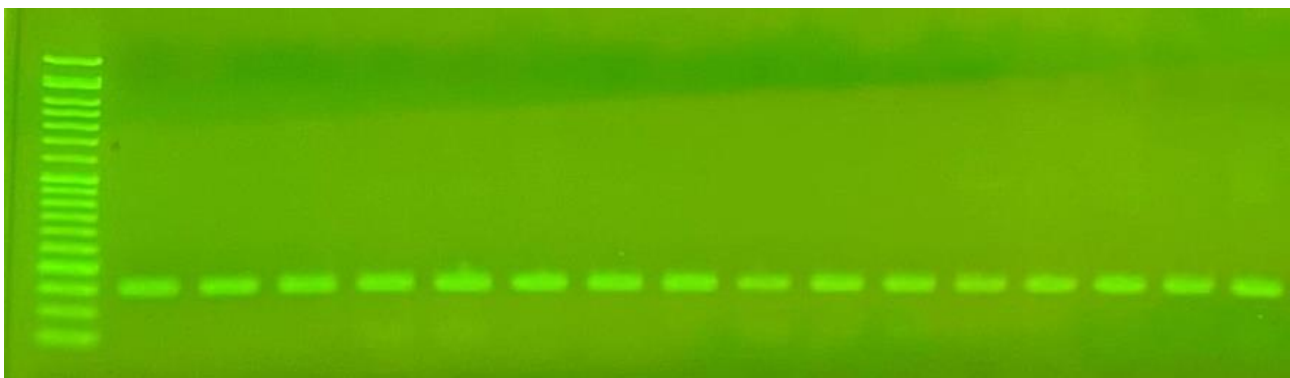In the figure below, there is the outcome of this procedure on the liver sample of *T.bernacchii:*

Figure 14: Treatments and controls of liver samples of *T. bernacchii*

3.7   Primer Design

To evaluate the gene expression of our target genesin specimens of *T. bernacchii*, primers must be designed according to our interests. For some genes, specific primers were already established:
Sod1, *sod2*, *gpx1*, *gpx3*, *gpx4*, *prdx3*, and *prdx5*.
While for *cat* and *prdx4,* a procedure to find them was necessary. Primers were designed on gene sequences available on the *NCBI GenBank® database*. After that, the Primer3 v 4.1.0 program was used to build them.
The parameters used to achieve that are listed in the table below.

Table 4: Parameters for building primers chosen.

Parameters	Level of interest
Primer Size Lenght	Min: 18, Max: 23-24 pb
Primer Tm (Melting Temperature)	Min: 60°C, Max: 67°C
The maximum difference between the melting temperatures of the two primers	2°C
Primer GC%	Max:60%
Range	100-150

IDT OligoAnalyzer™ tool was then used to analyse the primers, considering the following parameters listed in the table below.

Table 5: Parameters for analysing the primers.

Parameters	Choosed threshold
Probability of hairpin formation	ΔG < 3
Probability of intra-chain pairings within the single primer (self-dimer)	ΔG > -9
Probability of pairings between primer fw and primer rv (heterodimer)	ΔG > -9
Number of pairings at the 3' end	Not >3

To conclude this analysis, *Beacon DesignerTM* was used to verify the following characteristics:

- Cross-dimer (ΔG > -3.5);
- GC clamp (maximum 2).

If one primer could satisfy these parameters, it was then picked and used for further molecular analysis.

3.8   cDNA amplification

To verify that the designed primers were working, we amplified the cDNA obtained after DNase treatment through PCR. The quality of the *cDNA* was already assessed by control PCR with *β-actin*. The reagents and procedure for

PCR were described in point 3.X. If the outcome of this phase was positive, the primer was then tested on *qRT-PCR*.

In Figure 15, the outcome is shown for the liver sample using different primers of *prdx4*.
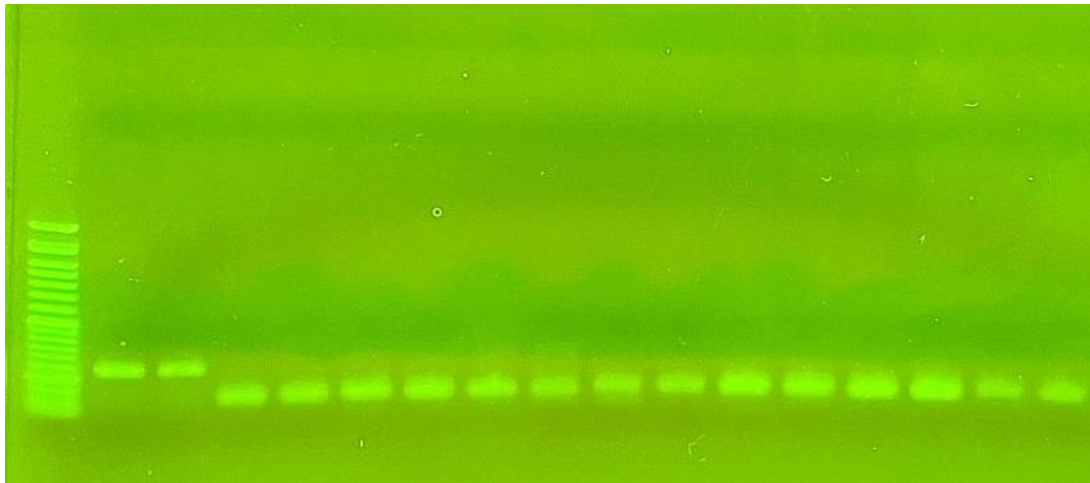

Figure 15: The First two bands were *β-actin*; all the others were primers of *prdx4*.

3.9 Gene expression analysis on qRT-PCR

For gene expression analysis, quantitative real-time PCR (qRT-PCR) was performed, which is the most powerful tool to carry out this analysis. qRT-PCR quantifies even slight differences in gene expression that can be very important in understanding biological processes and the mechanisms behind specific exposure effects or disease. A standard curve was generated for each gene to allow comparison between the Ct values of the samples and those of standards with known concentrations. The Ct (cycle threshold) corresponds to the cycle number at which the fluorescence of the amplified product crosses a manually set threshold, typically positioned around the midpoint of the exponential phase, where the quantity of DNA doubles with each cycle. The fluorescence emitted is proportional to the amount of cDNA that is amplified.

To generate the standard curve, a cDNA pool obtained from multiple individuals was used. This approach ensured the evaluation of primer efficiency across a range of genetic backgrounds and minimised individual-specific variation. The pooled cDNA was serially diluted to the following concentrations: 100 ng/µL, 50 ng/µL, 25 ng/µL, and 12.5 ng/µL. Each concentration was tested in 3 replicas. Only for the newly built primer was it necessary to assess the efficiency.

Table 6. Example of a dilution scheme on the RT plate to construct the standard curve.

Primer	cDNA concentrations (ng/µL)											
B-actin	100	100	100	50	50	50	25	25	25	12,5	12,5	12,5
PRDX4	100	100	100	50	50	50	25	25	25	12,5	12,5	12,5
CAT	100	100	100	50	50	50	25	25	25	12,5	12,5	12,5

Chemical dye SybrGreen was used, a fluorescent molecule capable of intercalating non-specifically into the minor groove of double-stranded *DNA.* As anticipated before, the fluorescence increases at each cycle since the amount of DNA increases as well. It was necessary to use a 96-well plate for the analysis. The amount of each component that must be used in each well is listed in the table below. Depending on the primers that must be used, it's necessary to prepare a new mix. (*cDNA* must be added after the mix in each well)

Table 7. Components for each well of the plate to perform qRT-PCR

Components	Volume (μL)
SybrGreen + ROX	5
Primer Forward	0.4
Primer Reverse	0.4
cDNA pool	2
PCR Grade Water	2.2

The following parameters were set for *qRT-PCR* (Figure 3.11):
- Initial denaturation: 2 min at 95 °C;
- 40 annealing and extension cycles: 20 s at 95°C and 60 s at 60 °C;
- Dissociation: 15 s at 95°C, 1 min at 60 °C, 15 s at 95°C, 15 s at 60 °C.

A slope of the calibration line equal to -3.5 represents the optimal efficiency (100%) of a primer. Among all the primers generated for each gene, only the best plus all the others of already known efficiency were used for subsequent qRT-PCR to detect differences between control and treated groups in liver and brain sample extracts.

Table 8. Primer list with melting temperature (Tm, °C). The last two are beta-actin.

Primer name	Sequence 5'$\Rightarrow$ 3'	Tm (°C)
Sod1 FW	TGCAAAGCTCAACATCACGGACA	60
Sod1 RV	CGTCCACCAGCATTGCCTGT	
Sod2 FW	GCCTCAGCCAAACTTTAAACCTGG	60
Sod2 RV	CATGGTGCTTGCTGTGGTGC	
Gpx1 FW	TGTACGGCACTTATCCAGACCAC	60
Gpx1 RV	AACGAGTTGGTTTCAGAGGATGC	
Gpx3 FW	GTGACTACAGGGGCAAGAGT	60
Gpx3 RV	GGAAAGCCGAGAATGGTGAG	
Gpx4 FW	CATCCTCGCCTTCCCTTCCAAC	60
Gpx4 RV	TGACTTTTCAGCCACTTCCACAGA	
Prdx3 FW	TGGACTTCTACTTCACCCAC	60
Prdx3 RV	ATCTGCTTGTTGAGGTCGGA	
Prdx4 FW	TGCTGTCTGACCTCACGCAC	60
Prdx4 RV	CGGGGAGATCGTTCATGGTGA	
Prdx5 FW	CCTGGAGCTTTTACCCCTGG	60
Prdx5 RV	ACAGAGATGCAAGCGACCTC	
Cat FW	CCATCTTCTTCATCAGGGACGCC	60
Cat RV	TGAGGCTCCAGAAGTCCCACA	

β-actin FW	AGGGTGTGATGGTCGGTATG	60
β-actin RV	CTTCTCCCTGTTGGCTTTGG	

The setup of the instrument was the same, so the procedure was the same to fill each well. The only difference was that each sample must be used on its own in a different well, and not in a pool of samples.

To calculate the gene expression level in the specimens, the ΔΔCt method was used. The Ct for each sample was normalised, subtracting the Ct of the housekeeping gene, which is *β-actin, and* by doing that, ΔCt was obtained. An additional calculation was performed, subtracting from all the treatment CT and control CT the mean of the CT of all controls, to obtain more reliable data. And now the ΔΔCt was obtained, for further better organisation and visualization of data, each value was elevated following the formula $2^{-\Delta\Delta Ct}$, which represents the final gene expression used on t-test between control and exposed group.

3.10 Superoxide dismutase activity

To quantify superoxide dismutase activity, an enzymatic assay was performed. The reaction rate was deduced by measuring the change in absorbance during the enzyme kinetics. The assay is based on the activity of xanthine oxidase, which catalyses the oxidation reaction of hypoxanthine to xanthine and then uric acid, causing the formation of free radicals, including superoxide ions. The latter, in the absence of SOD, act on cytochrome c^{3+}, reducing it to cytochrome c^{2+}; this determines a color variation and a consequent increase in absorbance. The SOD present in the sample, instead, dismutates the superoxide ions, preventing the reduction of cytochrome c^{3+}; in this case, however, a slight increase in absorbance is recorded, although much lower than the increase measured in the absence of this enzyme. Therefore, it is an indirect assay, based on the ability of the SOD enzyme to eliminate $\bullet O_2^-$ and consequently to inhibit the reactions caused by this radical.

Enzyme activity is expressed as U/mg of proteins, with one unit of SOD defined as the amount of enzyme that causes a 50% inhibition of the reduction reaction of oxidized cytochrome.

The following solutions were prepared:

- SOD buffer: 1,36 g of KH_2PO_4 in 200 mL of H_2O + 2,67 g $Na_2HPO_4 \times 2H_2O$ in 300 mL of H_2O + 0,019 g of EDTA + 0,033 g NaN_3 (pH 8,6);
- Hypoxanthine solution: 0,018 g in 8 mL of H_2O + 2 mL of NaOH (1 M);
- Cytochrome c solution (1,6 mM): 0,02 g in 1 mL of phosphate buffer;
- Xanthine oxidase solution: 100 µL of xanthine oxidase + 8 mL of H_2O.

Cuvettes were set up with the following composition, shown in Table 9.

Table 9. Composition of an example cuvette for SOD assay.

		SAMPLE	BLANK
REAGENTS	SOD buffer	930 µL	960 µL
	Hypoxanthine	20 µL	20 µL

	Cytochrome c	10 µL	10 µL
	Sample	30 µL	-
	Xanthine oxidase	10 µL	10 µL
TOTAL		1 mL	1 mL

The amount of sample to put in cuvettes is determined empirically based on the % inhibition of the colorimetric reaction, calculated with the following formula:

% inhibition = 100 − ((AS/AB) × 100)

AB = Δ blank absorbance   AS = Δ sample absorbance

To have significant data, the percentage of inhibition of the assay must be between 40 and 60%, in this way we are sure to be in the part of the Lambert-Beer graph in which the relationship between absorbance and concentration is linear.

Absorbance was measured at a wavelength of 550 nm at 10 s intervals for a total time of 3 minutes per sample. For each sample, the change in absorbance of a corresponding blank was measured; with this, the difference in the increase in absorbance during the reaction was calculated. The absorbance delta was read in the 30s (=0,5 min) interval, having the R^2 (which is an indicator of the goodness of fit to a linear model) as much as possible close to 1.

(The concentration of SOD in the sample was measured, using the Lambert-Beer law:

$$(U\ SOD/mL) = ((AB-AS)/AB) /0.5$$

- The result of the activity was multiplied by the sample dilution factor:

$$(U\ SOD/mL) \times 1/VS\ (mL)$$

- The result was divided by the total protein content of the sample, to normalise the SOD units to mg of total proteins:

$$U\ SOD/mg\ of\ proteins = \frac{(U\ SOD/mL)}{(mg\ proteins/mL)}$$

3.11 Catalase activity

Aebi's (1984) method was used to quantify catalase activity. Catalase works by reducing hydrogen peroxide to water, producing oxygen in the process. The rapid decomposition of H_2O_2 can be deduced directly from the decrease in absorbance, read at a wavelength of 240 nm. The following solutions were prepared to carry out the assay:

- Phosphate buffer Na_2HPO_4 − NaH_2PO_4 (50 mM, pH 7.5).
- H_2O_2 solution: 170 µl of stock H_2O_2 (30%) in 50 mL of H_2O (absorbance < 1.18).

Quartz cuvettes were set up with the following composition (Table 10):

Table 10. Composition of cuvettes for the CAT assay.

REAGENTS		SAMPLE	BLANK
	Phosphate buffer	1970 µL	1970 µL
	Homogenization buffer	-	30 µL
	Sample	30 µL	-
	H₂O₂ solution	1000 µL	1000 µL
TOTAL		3 mL	3 mL

Enzymatic kinetics were followed every 5 seconds for a total time of 1 minute. For each sample, 2 replicates were performed.

- The amount of active enzyme was calculated with the Lambert-Beer law; the value was multiplied by the dilution factor and normalised per minute:

$$\frac{U\ CAT}{mL} = \left(\frac{(A_i - A_f)}{40/0.833}\right) * \left(\frac{Total\ V}{V_{\{sample\}}}\right) * 1000$$

- The amount of enzyme has been normalised according to the amount of total proteins present in the sample:

$$\frac{U\ CAT}{mg\ proteins} = \frac{\left(\frac{U\ CAT}{mL}\right)}{\left(\frac{mg\ proteins}{mL}\right)}$$

3.12 Se-Glutathione peroxidases activity

The GPx assay is based on the reduction of hydroperoxides by glutathione peroxidase (GPx), which uses reduced glutathione (GSH) as an electron donor, converting it to oxidised glutathione (GSSG). This reaction is coupled to the regeneration of GSH from GSSG by glutathione reductase (GR), which uses NADPH as a reducing agent. During this process, NADPH is oxidised to NADP⁺, leading to a decrease in absorbance. GPx activity, which is directly proportional to the rate of NADPH consumption, was determined by monitoring the change in absorbance over time using a spectrophotometer. On the other hand, in the absence of *GPx*, *NADPH* is not oxidised; therefore, only a slight variation in absorbance is recorded, which is less than the decrease observed in the presence of *GPx*. Hydrogen peroxide was used as the substrate; therefore, the activity of only selenium-dependent *GPx* was evaluated.

The following solutions were prepared:

- Stock solution: 0.0062 g of *NADPH* (0,15 mM) + 0.019 g of *GSH* (2,5 mM) + 0.002 g of *NaN₃* (1,25 mM) + 52.5 µL of *GR* in 25 mL of phosphate buffer (125mM).
- H_2O_2 solution: 14 µL of stock H_2O_2 (30%) in 50 mL of H_2O (absorbance at 240 nm > 0,106).

Samples were analysed in two replicates; 2 blanks were measured for the whole analysis. Cuvettes were set up as in Table 11.

Table 11. Composition of cuvettes for GPx assay.

		SAMPLE	BLANK
REAGENTS	Stock solution	800 µL	800 µL
	Phosphate buffer	90 µL	100 µL
	Sample	10 µL	-
	H2O2 solution	100 µL	100 µL
TOTAL		1 mL	1 mL

The absorbance was read at a wavelength of 340 nm, at regular intervals of 60 s, for a total time of 300 s. The delta of absorbance in the total 5-minute trace was considered. *GPx* units per mg of total proteins were calculated as follows:

- The normalized absorbance variation on the blank was calculated:
  Δ = A-B
- The enzymatic activity of *GPx* was calculated with the Lambert-Beer law, per minute, per unit of volume:

$$\text{U GPx/mL} = \left[\frac{(Ai - Af)}{\frac{\Delta t}{6,22}}\right] \times \frac{1000}{V\ sample}$$

- The result was normalized to the mg of total protein present in the sample:

$$\text{U GPx/mg proteins} = \frac{(\text{U GPx/mL})}{(mg\ proteins\ /\ mL)}$$

3.13 Lipid peroxidation

Lipid Peroxidation Assay kit (Colorimetric/Fluorometric) was used to quantify lipid peroxidation. In this kit, lipid peroxidation is determined by the reaction of malondialdehyde (MDA) with thiobarbituric acid (TBA) to generate an *MDA-TBA* adduct; this can be quantified by colourimetric analysis, reading the absorbance at 532 nm, proportional to the concentration of *MDA*.

Reagent Preparation:

1. SDS Solution

The *SDS (sodium dodecyl sulfate)* solution may develop precipitates over time a dissolution procedure might be needed.

2. 1X TBA Acid Diluent

To prepare the *1X TBA (thiobarbituric acid)* acid diluent is needed to dilute the 2X stock solution with an equal volume of distilled or deionized water.

3. TBA Reagent *(to be prepared immediately before use)*

208 mg of thiobarbituric acid must be dissolved in 28.3 mL of the $1\times$ TBA acid diluent prepared as above. After dissolution, 1.7 mL of sodium hydroxide solution must be added and mixed to obtain a homogeneous solution.

Preparation of Stock Solutions: 10 µL of the MDA Standard combined with 597 µL of deionised water to obtain a 0.1 M MDA stock solution and mix it. Then, 10 µL of the 0.1 M stock solution was added to 990 µL of deionised water to prepare a 1 deionised water to prepare a 1 mM MDA working stock solution.

Preparation of the Dilution Series:

First, label nine microcentrifuge tubes from #1 to #9 (Table 12). Then add 875 µL of deionised water to tube #1, and 250 µL of deionised water to each of tubes #2 through #9. Add 125 µL of the 1 mM MDA stock to tube #1, mix thoroughly, and then briefly centrifuge. This yields Standard 1. Serial dilutions must be performed by transferring 250 µL from tube #1 to tube #2, mixing thoroughly each time before transferring the mixture to the next tube, and continuing this process until tube #8. Tube #9 is used as a blank and should contain onlydeionised water.

Table 12. Standard tubes distribution for lipid peroxidation assay.

Standard Tubes	1mM MDA Stock (µL)	Water (µL)	MDA Standard (µM)
1	125µL	875µL	125
2	250µL of Tube #1	250µL	62.5
3	250µL of Tube #2	250µL	31.25
4	250µL of Tube #3	250µL	15.63
5	250µL of Tube #4	250µL	7.81
6	250µL of Tube #5	250µL	3.91
7	250µL of Tube #6	250µL	1.95
8	250µL of Tube #7	250µL	0.98
9	0µL	250µL	0

Sample preparation:

A 100X BHT solution was added to the lysis buffer (e.g., 10 µL per 1 mL of buffer). For adherent cells, the culture medium was removed, and cells were washed twice with cold *1X PBS*. Then centrifuge at 1,000 × g for 10 minutes. After complete removal of PBS, cells were lysed at a concentration of 2×10^7 cells/mL in *BHT-containing lysis buffer*. Lysates were transferred to microcentrifuge tubes, resuspended by pipetting, and incubated at 2–8 °C for 30 minutes. Samples were then centrifuged again at 14,000 × g for 10 minutes at 2–8 °C.

Assay Procedure:

First, 100 µL of either sample or MDA standard was transferred into microcentrifuge tubes, followed by the addition of 100 µL of *SDS solution*. After thorough mixing and a brief centrifugation, the tubes were incubated at room temperature for 5 minutes. Subsequently, 250 µL of freshly prepared *TBA* reagent was added to each tube. Samples were mixed and incubated at 95 °C for 60 minutes. After incubation, tubes were placed on ice for 5 minutes and then centrifuged at 1,600 × g for 10 minutes. Finally, 200 µL of supernatant from each tube was transferred to a 96-well microplate, and the absorbance was measured immediately at 532 nm.

Calculations:

The normalised absorbance was calculated by subtracting the mean absorbance value of the blank from all the means of sample and standard readings. Background values can be significant and must be subtracted from all readings. The amount of MDA present in the samples may be determined from the standard curve. For each standard, the normalised absorbance was plotted against the Standard concentrations of MDA to obtain the linear equation and the slope of the standard curve. Using the standard curve, the quantity of MDA in nanomoles was determined for each sample. The concentration of MDA in the sample was then calculated as:

$$\text{Concentration of MDA (nmol/mL)} = \left(\frac{Sa}{Sv} \right) \text{x DF}$$

Where:
- SA: amount of MDA in sample (nmol) as determined from the standard curve

- SV: sample amount (mg) added into wells

- DF: sample dilution factor

3.14 Morphological indexes (HSI) and Fulton Condition Factor (FCF)

After each exposure time, fish were randomly sampled from the control and experimental groups, respectively. The fish were weighed and measured in length, and their livers were excised and weighed.

Hepato-somatic index (HIS) and Fulton Condition Factor (FCF) were thus calculated using the following formulas:

$$SSI = ((\text{spleen weight (g)}/(\text{total body weight (g)} - (\text{gonads weight (g)}) * 100$$

$$FCF = ((total\ weight(g)/\ (total\ lenght(cm)\ ^3)\ * 100$$

Gonad weight was removed from total body weight calculations to exclude possible bias due to differences in the maturity stage of the female gonads (Pham and Nguyen, 2019).

3.15 Statistical Analysis

1. Tool and program used:

- *Graph-Pad Prism* (Main instrument)

- *R-studio*

- *Excel*

2. Normality of the data:

To ensure that the data follow a normal distribution, a *Shapiro-Wilk Test* was carried out.

. H_0 (null hypothesis): The data are typically distributed.
. H_1 (alternative hypothesis): The data are not normally distributed.

According to this hypothesis, if the p-value is greater than 0.05, the data follow a normal distribution, and we reject the alternative hypothesis.

3. The independence of the data was assumed experimentally.

4. Since our data did not have equal variance, it was necessary to use *Welch's t-test* instead of a standard t-student test, which instead assumes it

5. *Welch's t-test two-sided* (Since the direction of the potential difference between the data was not known) was used on the analysis of differences between the control and treated group across the whole study. The threshold was set at α=0.05. The asterisk follows the results shown in Figure x.

4. Results

4.1   Liver results

4.1.1 Enzymatic Activities

Assay results showed a non-significant increase in the activity of the enzyme *SOD* (Figure 16A) in treated vs control. *CAT* activity is significantly down-regulated in the exposed group compared to the control (-37,45%, *p*-value = 0,033) (Figure 16B). Last, *Se-GPX* (Figure 16C) activity is increased in the treated group compared to the control but not in a significant way.
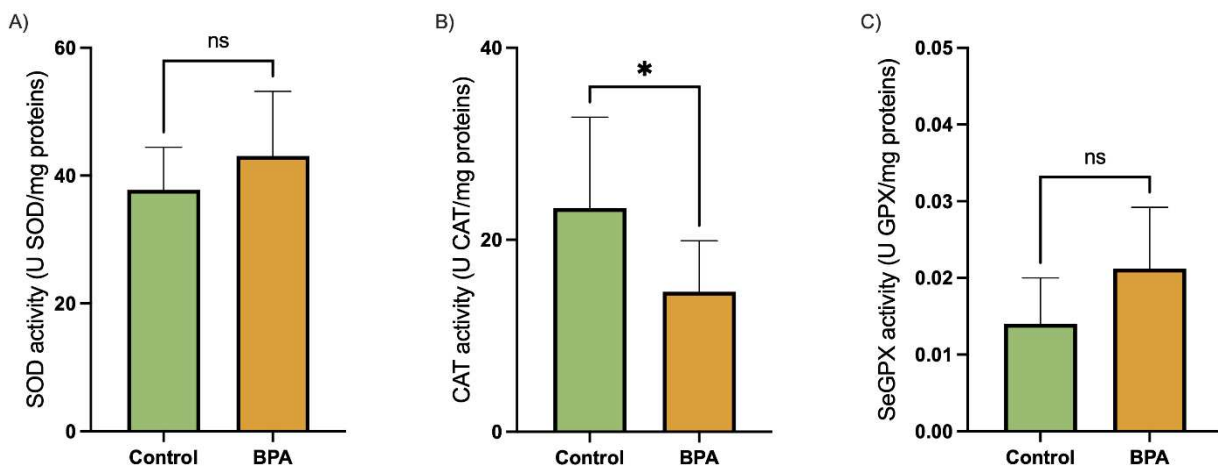

Figure 16. SOD activity (Fig. 16A), CAT activity (Fig. 16B) and Se-GPX activity (Fig. 16C) in *Trematomus bernacchii* liver in controls (green bars) and exposed groups (25 µg/L of BPA for 10 days; orange bars). Each enzyme activity is expressed as units of the enzyme per milligram of protein (U/mg protein) and presented as mean ± standard error of the mean (SEM). Significant differences are indicated by asterisks (*t*-tests) * (*p* < 0.05), ** (*p* < 0.01), *** (*p* < 0.001) and *ns* (*p* > 0.05).

4.1.2 Gene expression results in Liver:

Regarding mRNA expression levels, the qPCR results show a similar pattern to the enzymatic activity. SOD activity did not show significant changes, neither did *sod1* or *sod2* mRNA expressions. Regarding the key glutathione peroxidases isoforms investigated, *gpx3* shows a significant increase in the expression (+206.5%, *p*-value 0,029) while *gpx4* (+ 216%, *p*-value 0,035) in treated vs control, which may explain the increase in the activity of the biochemical assays. The *cat* is downregulated (-66.67%, *p*-value 0,0014) in the treated group, and this result is consistent with the enzymatic assay. For *prdxs*, there are different results. *Prdx3* is up-regulated (+133%, p-value 0,043) and *prdx4* is down-regulated (-57%, *p*-value 0,0043) in treatments. Regarding *prdx5*, there are no significant differences.
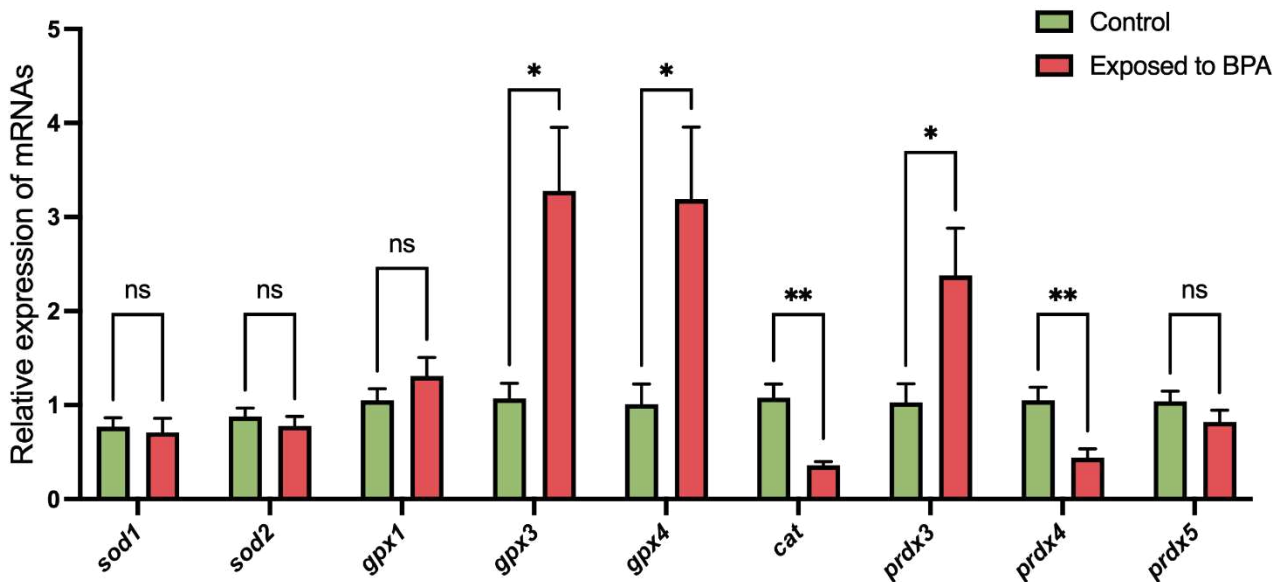
Figure 17. Relative expression of *sod1, sod2, gpx1, gpx3, gpx4, cat, prdx3, prdx4* and *prdx5* in the liver of exposed and control adult specimens of *T. bernacchii*. The mRNA values of the exposed groups (25 µg/L of BPA for 10 days; red bars) are presented compared to those of the control groups (green bars). Gene expressions are normalised to *beta actin* and are presented as mean ± standard error of the mean (SEM). Asterisks indicate statistical significance (*t*-tests) * ($p < 0.05$), ** ($p < 0.01$), *** ($p < 0.001$), and *ns* ($p > 0.05$).

4.1.3 Lipid Peroxidation:

There were no statistically significant differences in the lipid peroxidation observed in malondialdehyde (MDA) levels between the control and the exposed groups. However, the MDA levels detected through the assay show a weak increasing tendency in the exposed group compared to the control.
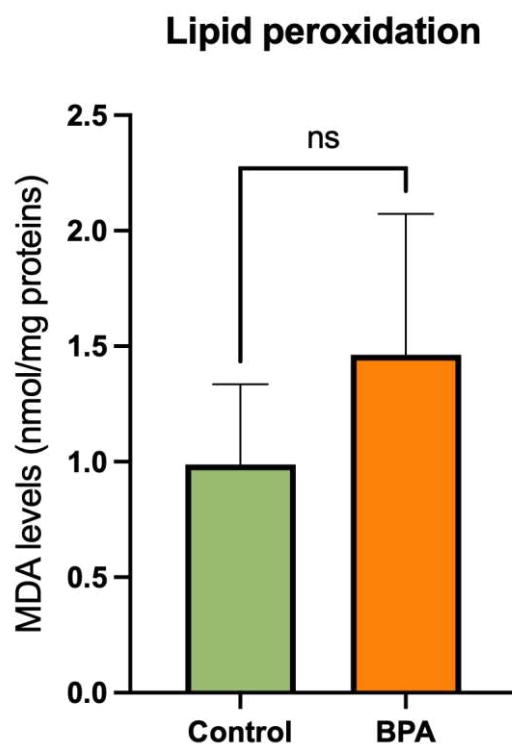

Figure 18) Lipid peroxidation levels in the livers of controls (green bars) and exposed groups (25 µg/L of BPA for 10 days; orange bars). Lipid peroxidation is expressed as nmol of MDA per milligram of protein (nmol/mg protein) and presented as mean ± standard error of the mean (SEM).

4.1.4 Hepato Somatic Index (HSI):

The dimensions of the liver increased in a strongly significant manner in the exposed group compared to the control (+47%, *p*-value <0.001). To avoid possible noise in the data, everything was normalised according to the total weight of the fish minus the gonad weight.
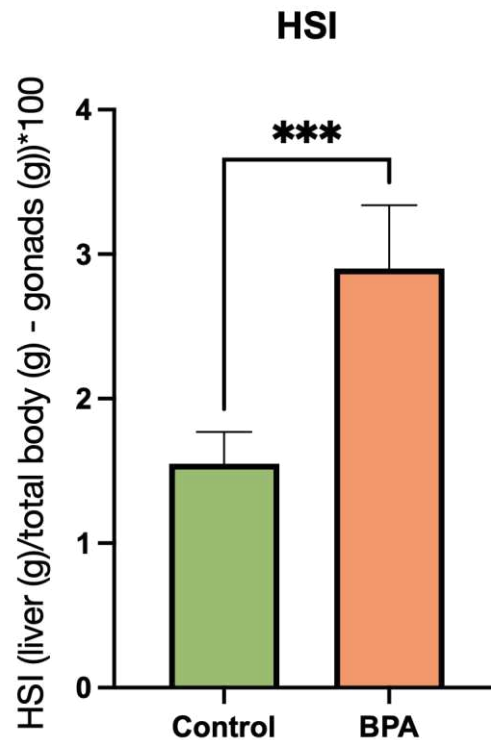

Figure 19. HSI (A) mean values referred to *T. bernacchii* specimens from the control groups in controls (green bars) and exposed groups (25 µg/L of BPA for 10 days; orange bars). Both HSI and SSI are expressed as ((liver weight (g) - gonad weight (g))/total body weight (g)) and ((spleen weight (g) - gonad weight (g))/total body weight (g)), respectively. Significant differences (*p* < 0.05) are indicated by distinct letters (two-way ANOVA).

4.2   Brain results

4.2.1 Enzymatic Activities

There is a downregulation of the enzyme SOD activity (-32.3%, p-value 0.009) in the treated group compared to the controls. The CAT activity during the assay was very low in both groups, and in fact, there are no significant differences. For Se-GPX, there is a strong downregulation in the treated group compared to the control one (-61%, p-value < 0.001).
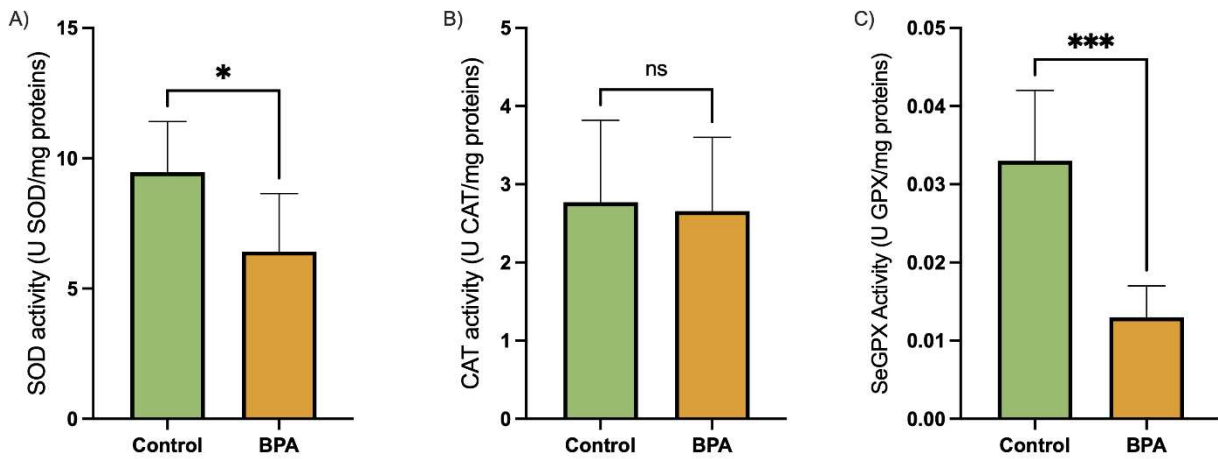
Figure 20. SOD activity (Fig. 20A), CAT activity (Fig. 20B) and Se-GPX activity (Fig. 20C) in *Trematomus bernacchii* brain in controls (green bars) and exposed groups (25 µg/L of BPA for 10 days; orange bars). Each enzyme activity is expressed as units of the enzyme per milligram of protein (U/mg protein) and presented as mean ± standard error of the mean (SEM). Significant differences are indicated by asterisks (*t*-tests) * ($p < 0.05$), ** ($p < 0.01$), *** ($p < 0.001$) and *ns* ($p > 0.05$).

4.2.2 Gene expression results in the Brain:

Even in this case, the molecular results resemble the biochemical assay outcomes. *Sod1* is downregulated in the treated group compared to controls (-49.5%, p-value 0.004), while *sod2* shows no significant differences. These results are in accordance with the biochemical outcome as anticipated before. *gpxs* are all downregulated in the treated group compared to the control, with varying decreases depending on the isoform. *gpx1* (-39.8%, p-value 0.047), *gpx3* (-62%, p-value 0.0029), *gpx4* (-58%, p-value 0.0027). CAT, as well as biochemistry, showed no significant differences. *Prdxs* analysed are all downregulated in the treated vs the control. *prdx3* (-52.3%, p-value 0.0057), *prdx4* (-52.2%, p-value 0.001), *prdx5* (-52.6%, p-value 0.006)
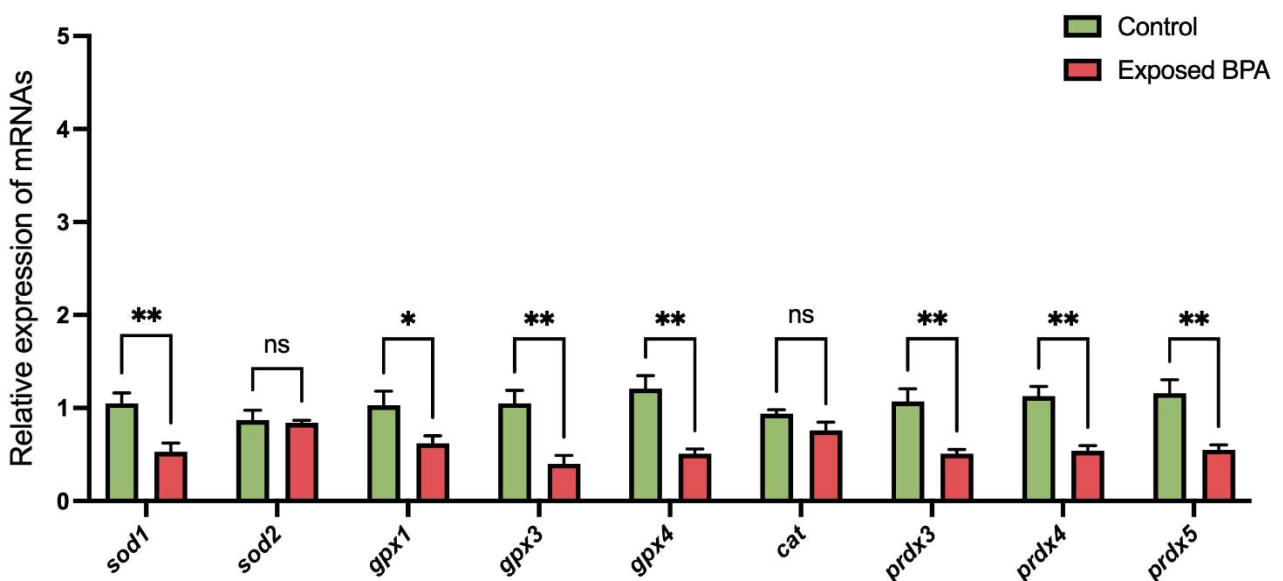

Figure 21. Relative expression of *sod1, sod2, gpx1, gpx3, gpx4, cat, prdx3, prdx4* and *prdx5* in the brain of exposed and control adult specimens of *T. bernacchii*. The mRNA values of the exposed groups (25 µg/L of BPA for 10 days; red bars) are presented compared to those of the control group (green bars). Gene expressions are normalised to *beta actin* and are presented as mean ±

standard error of the mean (SEM). Asterisks indicate statistical significance (t-tests) * ($p < 0.05$), ** ($p < 0.01$), *** ($p < 0.001$), and ns ($p > 0.05$).

4.3   Fulton's condition factor

Fulton's condition factor is a general index of overall body condition, which considers body weight relative to length. The analysis turned out to be non-significant when comparing the treated group to the control group, as well as the treated group to the control group of exposed specimens.
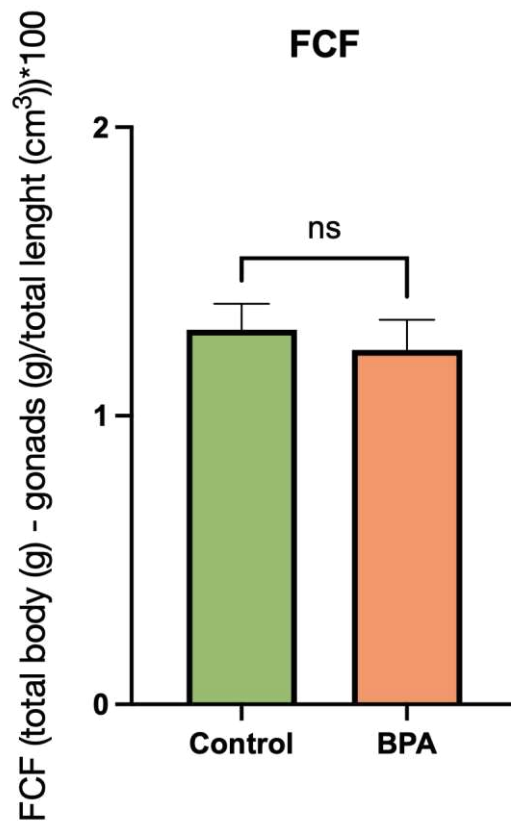

Figure 22. Fulton's condition factor in specimens of T.bernacchi exposed to BPA (25 µg/L of BPA for 10 days; orange bar) vs control conditions (green bar). Asterisks indicate statistical significance (t-tests) * ($p < 0.05$), ** ($p < 0.01$), *** ($p < 0.001$), and ns ($p > 0.05$).

5. Discussion

This study aimed to assess the antioxidant responses of the Antarctic fish *Trematomus bernacchii* when exposed to bisphenol A (BPA) at concentrations representative of a spill or of potential future contamination scenarios linked to global change. Oxidative stress is a key pathway through which pollutants, such as BPA, exert toxic effects, particularly in organs with high metabolic demand, such as the liver and brain. Our analysis was therefore focused on these two key organs. The liver was selected because it is a primary site of xenobiotic accumulation, due to its high lipid content (Jian et al., 2025). The brain, instead, was considered firstly as the first organ that perceives the stressor and activates the neuroendocrine cascades in teleosts (Schreck et al., 2016), and secondly due to the specific mode of action of BPA, which can cross the blood–brain barrier, and impact neurological development and behaviour (Kim et al., 2020). Being a lipophilic compound, like many other persistent pollutants, BPA can accumulate in neural tissues once it enters the brain (Khadrawy et al., 2016). Biochemical assays and expression analysis were conducted to evaluate the ability of *T. bernacchii* to maintain homeostasis in response to the increased reactive oxygen species (ROS) production resulting from BPA exposure (Ooe et al., 2005).

The combined analysis of gene transcription and enzyme activities consistently showed that mRNA expression patterns were mirrored by the biochemical results, suggesting a limited or almost absent post-transcriptional regulation at these experimental conditions. Notably, some responses were conserved across both organs, whereas others revealed striking tissue-specific divergences, which underscore the differential susceptibility of the liver and brain to BPA exposure. BPA possess diverse mechanisms of action related to the impacted pathway (Wetherill et al., 2007; Yang et al., 2023).

In the liver, catalase activity was significantly affected by the treatment, with a reduction observed in the treated group compared to the control group. This decrease was supported by qRT-PCR data, which revealed a significant downregulation of *cat* expression in exposed fish. Since CAT is localised in peroxisomes, the simultaneous reduction in both transcription and enzyme activity indicates a potential site-specific impairment, suggesting that these organelles may be directly targeted by BPA toxicity (Terlecky et al., 2006). However, the observed downregulation could represent an energy-saving strategy, with the organism which invests its resources in other antioxidants to maintain homeostasis. Interestingly, similar patterns of enzyme modulation have been described in humans under pathological conditions such as Alzheimer's disease (Chandrasekaran et al., 1996). One of these could be PRDX5, which is also expressed in peroxisomes and retains its gene expression under our experimental conditions. Unfortunately, it was not possible to analyse the

enzymatic activity for this protein, so we could not verify whether increased biosynthesis occurs as a result of post-transcriptional regulation.

About the other PRDX isoforms, the increased expression of *prdx3* (an enzyme specifically expressed in mitochondria) suggests an increase in BPA-induced H_2O_2 production in this organelle. Interesting is the downregulation of *prdx4*. This isoform is expressed explicitly in the endoplasmic reticulum and extracellular environment (Lee, 2020; Valero et al., 2015). Therefore, it protects against oxidative damage by removing ROS both inside and outside the cell (Yamada and Guo, 2018) In the endoplasmic reticulum, it performs two main functions: it acts as a scavenger against peroxides and inhibits lipid accumulation in the cell (Yamada and Guo, 2018). Through the down-regulation of the prdx4 gene, the inhibition of lipid accumulation in the cell is thus prevented, initiating the process of vacuolization and a condition known as steatosis. Our liver samples were not analysed histologically for evidence of steatosis, but we cannot exclude the possibility that BPA exposure has this effect in our fish, as has been amply demonstrated in mammals (Hong et al., 2023; Li et al., 2025; Zhang et al., 2024) In support of this hypothesis, the hepatosomatic index (HSI) showed a highly significant increase in the treated group compared to the control group. It remains to be clarified whether hepatic steatosis is a condition that increases the vulnerability of this organ or whether it is a defence mechanism against BPA toxicity, similar to other environmental contaminants such as PFAS (Pacchini et al., 2025; Piva et al., 2022).

This increase in liver mass may also indicate a possible inflammatory response, although this aspect was not directly assessed in the present study. Future analyses of cyclooxygenase activity and prostaglandin production may provide more definitive evidence of inflammation. Similar liver alterations, including fibrosis and inflammation, have been reported in other species after exposure to BPA, such as rats (Elswefy et al., 2016) and carp (Faheem et al., 2016), highlighting the potential relevance of this response in *T. bernacchii*. However, a reduction in *prdx4* expression would contradict this hypothesis, as an inflammatory response should also involve an increase in the presence of anti-oxidant enzymes in the extracellular environment, such as PRDX4. Nevertheless, our results showed increased expression levels of *gpx3, an enzyme known to counteract oxidative stress associated with* the inflammatory state in mammals (Qiao et al., 2025).

In addition to *gpx3*, *gpx4* was also significantly upregulated in treated fish, further supporting the previously proposed mitochondrial oxidative stress hypothesis, as this enzyme is expressed specifically in mitochondria (Pei et al., 2023). However, it should be noted that while there is an increase in the transcription of genes encoding GPX, there is no statistically significant increase in the corresponding tissue enzyme activity. This is likely because the risk of oxidative stress was relatively low, as evidenced by the levels of lipid peroxidation remaining almost unchanged in the treated group compared to the controls. The lack of translation of the neosynthesised messengers is probably

due to a post-transcriptional regulation mediated by the stress granules (Piva et al., 2024).

In the liver, superoxide dismutase (SOD) activity also remains unchanged, which is consistent with the unaltered expression of both *sod1* and *sod2*. Therefore, this result seems to indicate that exposure to BPA results in no change in the rate of superoxide anion formation, the specific target of these enzymes.

Overall, these results reflect a compensatory response between the different enzymatic components of the antioxidant system. Similar patterns of antioxidant gene regulation under BPA stress have also been reported in *Oryzias latipes* (Qiu et al., 2016) and salmon. Both upregulation and downregulation of antioxidant genes in response to BPA exposure have been observed in previous studies (Kaya and Kaptaner, 2016), suggesting that such responses are species- and context-dependent.

This compensation, in addition to demonstrating significant plasticity, is intended to preserve cellular homeostasis under these exposure conditions and maintain the health of T. bernacchii. A state of well-being confirmed by the Fulton's condition factor, which remains constant between 1.1 and 1.3. However, the observed trends raise concerns for future scenarios involving higher BPA concentrations or longer exposure durations. Under such conditions, these compensatory responses may be insufficient to protect the lipid profile and maintain redox balance, potentially leading to oxidative stress and, ultimately, mortality in exposed individuals.

In sharp contrast, brain tissue exhibited a substantial reduction in SOD and GPX activity, accompanied by a downregulation of nearly all the genes analysed. However, we cannot refer to a condition of profound oxidative stress. In fact, CAT activity levels remain unchanged following BPA treatment, as does *sod2* and *cat* mRNA expression, indicating that at least peroxisomes and mitochondria maintain their active antioxidant defences.

The significant decrease in Se-GPX activity was consistent with qRT-PCR results, which showed a substantial downregulation of all the *gpx* genes considered (*gpx1, gpx3, gpx4*) in the treated group, and overall suggests a possible toxicity effect, albeit at an early stage. GPX1 is ubiquitously expressed in the cytosol of virtually all cells, suggesting that its reduction may reflect a general toxicity effect induced by BPA exposure. Similar general toxic effects have been reported in humans (Ahmad et al., 2024) and in other fish species (Faheem and Lone, 2018). GPX3 is mainly secreted into the extracellular fluid and plasma; its reduction in the brain could indicate either a decreased requirement for this protein or vascular-level damage, as also observed in other fish species (Wang et al., 2019). GPX4 is typically localised in both the cytosol and mitochondria, and its downregulation supports the hypothesis of mitochondrial damage.

Also SOD activity was significantly reduced following BPA exposure. At the transcriptional level, the decrease in *sod1* mRNA is probably sufficient to explain the observed reduction in overall SOD activity, as *sod2* expression remained unaffected. The decline in *sod1* is likely enough to justify the observed reduction in overall SOD activity. Similar BPA-related reductions in *sod* expression have also been described in humans (Hassan et al., 2012). The expression of sod2 remains unchanged, suggesting that, as previously hypothesised in the liver, BPA is unable to induce superoxide anion production at the mitochondrial level in the brain.

In contrast, biochemical analysis showed that CAT activity did not differ significantly between treated and control groups, with nearly identical values in both conditions. This finding was consistent with qRT-PCR results, where *cat* expression also remained unchanged, showing only a slight, non-significant decrease in the treated group. Since previous studies have shown that high levels of H2O2 can inhibit CAT activity (Lardinois et al., 1996) these data suggest that peroxisomes are not affected by a significant increase in ROS production.

In the brain, all PRDX isoforms analysed (*prdx3, prdx4, prdx5*) were also significantly downregulated, indicating a generalised reduction in H_2O_2 detoxification capacity across mitochondria, ER, and peroxisomes. To date, no studies have investigated *Prdx expression under BPA exposure, making these results novel and* highlighting the need for further investigation. For example, due to limited tissue availability, it was not possible to study lipid oxidation in this tissue. However, their downregulation in the brain, together with that of genes encoding GPX and SOD1, suggests a higher vulnerability to oxidative damage in neuronal tissues, consistent with the brain's known sensitivity to redox imbalance. Downregulation of antioxidant genes after BPA exposure was also found in salmon (Yazdani et al., 2016).

6. Conclusions

This study expands our understanding of the potential toxic effects of BPA exposure in the Antarctic fish *T. bernacchii*, with a particular focus on its antioxidant defence system. The findings raise serious concerns about this contaminant, whose production continues to grow and whose presence is becoming increasingly widespread worldwide, including in the Antarctic region. The results also reveal clear tissue-specific responses to BPA exposure.

Among the two organs analysed, the liver appeared to be the least affected, likely due to its inherent capacity to metabolise and eliminate xenobiotics. Under the experimental timeframe and conditions, oxidative stress can essentially be ruled out in this organ. Nevertheless, the data suggest the possibility of an inflammatory response in the liver, which warrants further investigation.

In contrast, the brain was markedly affected by BPA toxicity, confirming the ability of this compound to cross the blood–brain barrier. All controls, as confirmed by qRT-PCR. While such effects may not directly translate into increased mortality rates, brain impairment could significantly alter essential behaviours such as feeding, mating, and predator avoidance, ultimately affecting the species' ecological fitness.

At the subcellular level, the most striking effect appears to be potential mitochondrial damage, which could lead to localised increases in ROS no longer adequately counteracted by antioxidant enzymes.

Overall, *T. bernacchii* exhibits a certain degree of plasticity in its ability to mitigate ROS, particularly in the liver. However, specific tissues such as the brain remain highly vulnerable to BPA-induced damage, raising concerns about the resilience of this species to future environmental stressors.

To conclude, this study offers valuable insights that can inform policymakers about the toxic effects of BPA and the potential risks associated with increasing concentrations of this contaminant in relatively pristine environments, such as Antarctica. These findings underscore the urgent need to reconsider and potentially reduce the industrial use of BPA to protect vulnerable ecosystems.

7. Bibliography

Abouelenein, D., Mustafa, A.M., Nzekoue, F.K., Caprioli, G., Angeloni, S., Tappi, S., Castagnini, J.M., Dalla Rosa, M., Vittori, S., 2022. The Impact of Plasma Activated Water Treatment on the Phenolic Profile, Vitamins Content, Antioxidant and Enzymatic Activities of Rocket-Salad Leaves. Antioxidants 12, 28. https://doi.org/10.3390/antiox12010028

Ahmad, I., Kaur, M., Tyagi, D., Singh, T.B., Kaur, G., Afzal, S.M., Jauhar, M., 2024. Exploring novel insights into the molecular mechanisms underlying Bisphenol A-induced toxicity: A persistent threat to human health. Environ. Toxicol. Pharmacol. 108, 104467. https://doi.org/10.1016/j.etap.2024.104467

Alfonso-Prieto, M., Biarnés, X., Vidossich, P., Rovira, C., 2009. The Molecular Mechanism of the Catalase Reaction. J. Am. Chem. Soc. 131, 11751–11761. https://doi.org/10.1021/ja9018572

Atli, G., Canli, E.G., Eroglu, A., Canli, M., 2016. Characterization of antioxidant system parameters in four freshwater fish species. Ecotoxicol. Environ. Saf. 126, 30–37. https://doi.org/10.1016/j.ecoenv.2015.12.012

Bargagli, R., 2008. Environmental contamination in Antarctic ecosystems. Sci. Total Environ. 400, 212–226. https://doi.org/10.1016/j.scitotenv.2008.06.062

Bargagli, R., Rota, E., 2024. Environmental contamination and climate change in Antarctic ecosystems: an updated overview. Environ. Sci. Adv. 3, 543–560. https://doi.org/10.1039/D3VA00113J

Bargelloni, L., Marcato, S., Patarnello, T., 1998. Antarctic fish hemoglobins: Evidence for adaptive evolution at subzero temperature. Proc. Natl. Acad. Sci. 95, 8670–8675. https://doi.org/10.1073/pnas.95.15.8670

Benedetti, M., Nigro, M., Regoli, F., 2010. Characterisation of antioxidant defences in three Antarctic notothenioid species from Terra Nova Bay (Ross Sea). Chem. Ecol. 26, 305–314. https://doi.org/10.1080/02757541003789066

Biswal, A., Srivastava, P., N, S., Kumar, M., 2020. Plastic originated bisphenol A: A potential endocrine disruptor for fish reproduction. Int. J. Chem. Stud. 8, 2085–2089. https://doi.org/10.22271/chemi.2020.v8.i1ae.8573

Chandrasekaran, K., Hatanpää, K., Brady, D.R., Rapoport, S.I., 1996. Evidence for Physiological Down-regulation of Brain Oxidative Phosphorylation in Alzheimer's Disease. Exp. Neurol. 142, 80–88. https://doi.org/10.1006/exnr.1996.0180

Chen, L., DeVries, A.L., Cheng, C.-H.C., 1997. Evolution of antifreeze glycoprotein gene from a trypsinogen gene in Antarctic notothenioid fish. Proc. Natl. Acad. Sci. 94, 3811–3816. https://doi.org/10.1073/pnas.94.8.3811

Chowdhury, S., Saikia, S.K., 2020. Oxidative Stress in Fish: A Review. J. Sci. Res. 12, 145–160. https://doi.org/10.3329/jsr.v12i1.41716

Chown, S.L., Clarke, A., Fraser, C.I., Cary, S.C., Moon, K.L., McGeoch, M.A., 2015. The changing form of Antarctic biodiversity. Nature 522, 431–438. https://doi.org/10.1038/nature14505

Clarke, A., Barnes, D., Hodgson, D., 2005. How isolated is Antarctica? Trends Ecol. Evol. 20, 1–3. https://doi.org/10.1016/j.tree.2004.10.004

Dalrymple, P.C., 2013. A Physical Climatology of the Antarctic Plateau, in: Rubin, M.J. (Ed.), Antarctic Research Series. American Geophysical Union, Washington, D. C., pp. 195–231. https://doi.org/10.1029/AR009p0195

Deisseroth, A., Dounce, A.L., 1970. Catalase: Physical and chemical properties, mechanism of catalysis, and physiological role. Physiol. Rev. 50, 319–375. https://doi.org/10.1152/physrev.1970.50.3.319

Elswefy, S.E., Abdallah, F.R., Atteia, H.H., Wahba, A.S., Hasan, R.A., 2016. Inflammation, oxidative stress and apoptosis cascade implications in bisphenol A-induced liver fibrosis in male rats. Int. J. Exp. Pathol. 97, 369–379. https://doi.org/10.1111/iep.12207

Faheem, M., Jahan, N., Lone, K.P., 2016. HISTOPATHOLOGICAL EFFECTS OF BISPHENOL-A ON LIVER, KIDNEYS AND GILLS OF INDIAN MAJOR CARP, CATLA CATLA (HAMILTON, 1822). J Anim Plant Sci.
Faheem, M., Lone, K.P., 2018. Oxidative stress and histopathologic biomarkers of exposure to bisphenol-A in the freshwater fish, Ctenopharyngodon idella. Braz. J. Pharm. Sci. 53. https://doi.org/10.1590/s2175-97902017000317003

Franco-Belussi, L., Santos, L.R.D.S., Zieri, R., Vicentini, C.A., Taboga, S.R., Oliveira, C.D., 2012. Liver Anatomy, Histochemistry, and Ultrastructure of *Eupemphix Nattereri* (Anura: Leiuperidae) During the Breeding Season. Zoolog. Sci. 29, 844–848. https://doi.org/10.2108/zsj.29.844

Giltrap, M., Ronan, J., Bignell, J.P., Lyons, B.P., Collins, E., Rochford, H., McHugh, B., McGovern, E., Bull, L., Wilson, J., 2017. Integration of biological effects, fish histopathology and contaminant measurements for the assessment of fish health: A pilot application in Irish marine waters. Mar. Environ. Res. 129, 113–132. https://doi.org/10.1016/j.marenvres.2017.04.004

Griffiths, H.J., 2010. Antarctic Marine Biodiversity – What Do We Know About the Distribution of Life in the Southern Ocean? PLoS ONE 5, e11683. https://doi.org/10.1371/journal.pone.0011683

Han, Y., Liu, W., Hansen, H.Chr.B., Chen, X., Liao, X., Li, H., Wang, M., Yan, N., 2016. Influence of long-range atmospheric transportation (LRAT) on mono-to octa-chlorinated PCDD/Fs levels and distributions in soil around Qinghai Lake, China. Chemosphere 156, 143–149. https://doi.org/10.1016/j.chemosphere.2016.04.110

Hassan, Z.K., Elobeid, M.A., Virk, P., Omer, S.A., ElAmin, M., Daghestani, M.H., AlOlayan, E.M., 2012. Bisphenol A Induces Hepatotoxicity through Oxidative Stress in Rat Model. Oxid. Med. Cell. Longev. 2012, 1–6. https://doi.org/10.1155/2012/194829

Holm-Hansen, O., 1985. Nutrient Cycles in Antarctic Marine Ecosystems, in: Siegfried, W.R., Condy, P.R., Laws, R.M. (Eds.), Antarctic Nutrient Cycles and Food Webs. Springer Berlin Heidelberg, Berlin, Heidelberg, pp. 6–10. https://doi.org/10.1007/978-3-642-82275-9_2

Hong, T., Zou, J., He, Y., Zhang, H., Liu, H., Mai, H., Yang, J., Cao, Z., Chen, X., Yao, J., Feng, D., 2023. Bisphenol A induced hepatic steatosis by disturbing bile acid metabolism and FXR/TGR5 signaling

pathways via remodeling the gut microbiota in CD-1 mice. Sci. Total Environ. 889, 164307. https://doi.org/10.1016/j.scitotenv.2023.164307

Ighodaro, O.M., Akinloye, O.A., 2018. First line defence antioxidants-superoxide dismutase (SOD), catalase (CAT) and glutathione peroxidase (GPX): Their fundamental role in the entire antioxidant defence grid. Alex. J. Med. 54, 287–293. https://doi.org/10.1016/j.ajme.2017.09.001

Jacobs, S.S., Helmer, H.H., Doake, C.S.M., Jenkins, A., Frolich, R.M., 1992. Melting of ice shelves and the mass balance of Antarctica. J. Glaciol. 38, 375–387. https://doi.org/10.3189/S0022143000002252

Jian, Y., Li, Y., Zhou, Y., Mu, W., 2025. Pollutants in Microenvironmental Cellular Interactions During Liver Inflammation Cancer Transition and the Application of Multi-Omics Analysis. Toxics 13, 163. https://doi.org/10.3390/toxics13030163

Jomova, K., Raptova, R., Alomar, S.Y., Alwasel, S.H., Nepovimova, E., Kuca, K., Valko, M., 2023. Reactive oxygen species, toxicity, oxidative stress, and antioxidants: chronic diseases and aging. Arch. Toxicol. 97, 2499–2574. https://doi.org/10.1007/s00204-023-03562-9

Kaya, Ö., Kaptaner, B., 2016. Antioxidant defense system parameters in isolated fish hepatocytes exposed to bisphenol A — Effect of vitamin C. Acta Biol. Hung. 67, 225–235. https://doi.org/10.1556/018.67.2016.3.1

Khadrawy, Y.A., Noor, N.A., Mourad, I.M., Ezz, H.S.A., 2016. Neurochemical impact of bisphenol A in the hippocampus and cortex of adult male albino rats. Toxicol. Ind. Health 32, 1711–1719. https://doi.org/10.1177/0748233715579803

Kim, S.S., Hwang, K.-S., Yang, J.Y., Chae, J.S., Kim, G.R., Kan, H., Jung, M.H., Lee, H.-Y., Song, J.S., Ahn, S., Shin, D.-S., Lee, K.-R., Kim, S.K., Bae, M.A., 2020. Neurochemical and behavioral analysis by acute exposure to bisphenol A in zebrafish larvae model. Chemosphere 239, 124751. https://doi.org/10.1016/j.chemosphere.2019.124751

Kime, D.E., 1998. Disruption of Liver Function, in: Endocrine Disruption in Fish. Springer US, Boston, MA, pp. 201–246. https://doi.org/10.1007/978-1-4615-4943-7_9

Kristiansen, T.S., Fernö, A., Pavlidis, M.A., Van De Vis, H. (Eds.), 2020. The Welfare of Fish, Animal Welfare. Springer International Publishing, Cham. https://doi.org/10.1007/978-3-030-41675-1

Lardinois, O.M., Mestdagh, M.M., Rouxhet, P.G., 1996. Reversible inhibition and irreversible inactivation of catalase in presence of hydrogen peroxide. Biochim. Biophys. Acta BBA - Protein Struct. Mol. Enzymol. 1295, 222–238. https://doi.org/10.1016/0167-4838(96)00043-X

Lee, Y.J., 2020. Knockout Mouse Models for Peroxiredoxins. Antioxidants 9, 182. https://doi.org/10.3390/antiox9020182

Li, C.-L., Yao, Z.-Y., Zhang, Y.-F., Cui, X.-T., Sun, A., Cao, J.-Y., Wang, Z.-S., 2025. Bisphenols exposure and non-alcoholic fatty liver disease: from environmental trigger to molecular pathogenesis. Front. Endocrinol. 16, 1606654. https://doi.org/10.3389/fendo.2025.1606654

Lien, Y.-C., Feinstein, S.I., Dodia, C., Fisher, A.B., 2012. The Roles of Peroxidase and Phospholipase A₂ Activities of Peroxiredoxin 6 in Protecting Pulmonary Microvascular Endothelial Cells Against Peroxidative Stress. Antioxid. Redox Signal. 16, 440–451. https://doi.org/10.1089/ars.2011.3950

Liu, X., Shi, H., Xie, B., Dionysiou, D.D., Zhao, Y., 2019. Microplastics as Both a Sink and a Source of Bisphenol A in the Marine Environment. Environ. Sci. Technol. 53, 10188–10196. https://doi.org/10.1021/acs.est.9b02834

McCarthy, A.H., Peck, L.S., Hughes, K.A., Aldridge, D.C., 2019. Antarctica: The final frontier for marine biological invasions. Glob. Change Biol. 25, 2221–2241. https://doi.org/10.1111/gcb.14600

Mittler, R., 2017. ROS Are Good. Trends Plant Sci. 22, 11–19. https://doi.org/10.1016/j.tplants.2016.08.002

Nannenga, B.L., Shi, D., Hattne, J., Reyes, F.E., Gonen, T., 2014. Structure of catalase determined by MicroED. eLife 3, e03600. https://doi.org/10.7554/eLife.03600

Ooe, H., Taira, T., Iguchi-Ariga, S.M.M., Ariga, H., 2005. Induction of Reactive Oxygen Species by Bisphenol A and Abrogation of Bisphenol A-Induced Cell Injury by DJ-1. Toxicol. Sci. 88, 114–126. https://doi.org/10.1093/toxsci/kfi278

Pacchini, S., Vanzan, G., Schumann, S., Piva, E., Bakiu, R., Bertotto, D., Bottacin-Busolin, A., Irato, P., Marion, A., Santovito, G., 2025. Characterisation of the prdx4 gene in Squalius cephalus and its role in freshwater environments with varying impact of perfluoroalkyl substances (PFAS). Chemosphere 373, 144167. https://doi.org/10.1016/j.chemosphere.2025.144167

Pei, J., Pan, X., Wei, G., Hua, Y., 2023. Research progress of glutathione peroxidase family (GPX) in redoxidation. Front. Pharmacol. 14, 1147414. https://doi.org/10.3389/fphar.2023.1147414

Pham, H.Q., Nguyen, A.V., 2019. Seasonal changes in hepatosomatic index, gonadosomatic index and plasma estradiol-17β level in captively reared female rabbit fish (*Siganus guttatus*). Aquac. Res. 50, 2191–2199. https://doi.org/10.1111/are.14100

Piva, E., Nicorelli, E., Pacchini, S., Schumann, S., Drago, L., Vanzan, G., Tolomeo, A.M., Irato, P., Bakiu, R., Gerdol, M., Santovito, G., 2024. Unravelling stress granules in the deep cold: Characterisation of TIA-1 gene sequence in Antarctic fish species. Fish Shellfish Immunol. 154, 109903. https://doi.org/10.1016/j.fsi.2024.109903

Piva, E., Schumann, S., Dotteschini, S., Brocca, G., Radaelli, G., Marion, A., Irato, P., Bertotto, D., Santovito, G., 2022. Antioxidant Responses Induced by PFAS Exposure in Freshwater Fish in the Veneto Region. Antioxidants 11, 1115. https://doi.org/10.3390/antiox11061115

Puga, S., Pereira, P., Pinto-Ribeiro, F., O'Driscoll, N.J., Mann, E., Barata, M., Pousão-Ferreira, P., Canário, J., Almeida, A., Pacheco, M., 2016. Unveiling the neurotoxicity of methylmercury in fish (Diplodus sargus) through a regional morphometric analysis of brain and swimming behavior assessment. Aquat. Toxicol. 180, 320–333. https://doi.org/10.1016/j.aquatox.2016.10.014

Qiao, M., Zhang, L., Wu, Y., Ma, B., 2025. Glutathione peroxidase 3 antagonizes oxidative stress and inflammation in diabetic retinopathy via NrF2/NF-κB pathway. Int. Ophthalmol. 45, 231. https://doi.org/10.1007/s10792-025-03582-7

Qiu, W., Shen, Y., Pan, C., Liu, S., Wu, M., Yang, M., Wang, K.-J., 2016. The potential immune modulatory effect of chronic bisphenol A exposure on gene regulation in male medaka (Oryzias latipes) liver. Ecotoxicol. Environ. Saf. 130, 146–154. https://doi.org/10.1016/j.ecoenv.2016.04.015

Rhee, S.G., 2016. Overview on Peroxiredoxin. Mol. Cells 39, 1–5.
https://doi.org/10.14348/molcells.2016.2368

Schreck, C.B., Tort, L., Farrell, A.P., Brauner, C.J., 2016. Biology of stress in fish, Fish physiology.
Elsevier/AP, Academic Press is an imprint of Elsevier, Amsterdam Boston.
Sies, H., Berndt, C., Jones, D.P., 2017. Oxidative Stress. Annu. Rev. Biochem.
https://doi.org/10.1146/annurev-biochem-061516-045037

Soengas, J.L., Aldegunde, M., 2002. Energy metabolism of fish brain. Comp. Biochem. Physiol. B
Biochem. Mol. Biol. 131, 271–296. https://doi.org/10.1016/S1096-4959(02)00022-2

Terlecky, S.R., Koepke, J.I., Walton, P.A., 2006. Peroxisomes and aging. Biochim. Biophys. Acta BBA
- Mol. Cell Res. 1763, 1749–1754. https://doi.org/10.1016/j.bbamcr.2006.08.017

Timmermann, R., Beckmann, A., Hellmer, H.H., 2001. The role of sea ice in the fresh-water budget
of the Weddell Sea, Antarctica. Ann. Glaciol. 33, 419–424.
https://doi.org/10.3189/172756401781818121

Turner, J., Anderson, P., Lachlan-Cope, T., Colwell, S., Phillips, T., Kirchgaessner, A., Marshall, G.J.,
King, J.C., Bracegirdle, T., Vaughan, D.G., Lagun, V., Orr, A., 2009. Record low surface air
temperature at Vostok station, Antarctica. J. Geophys. Res. Atmospheres 114, 2009JD012104.
https://doi.org/10.1029/2009JD012104

Valero, Y., Martínez-Morcillo, F., Esteban, M., Chaves-Pozo, E., Cuesta, A., 2015. Fish
Peroxiredoxins and Their Role in Immunity. Biology 4, 860–880.
https://doi.org/10.3390/biology4040860

Valko, M., Izakovic, M., Mazur, M., Rhodes, C.J., Telser, J., 2004. Role of oxygen radicals in DNA
damage and cancer incidence. Mol. Cell. Biochem. 266, 37–56.
https://doi.org/10.1023/B:MCBI.0000049134.69131.89

Vecchiato, M., Argiriadis, E., Zambon, S., Barbante, C., Toscano, G., Gambaro, A., Piazza, R., 2015.
Persistent Organic Pollutants (POPs) in Antarctica: Occurrence in continental and coastal surface
snow. Microchem. J. 119, 75–82. https://doi.org/10.1016/j.microc.2014.10.010

Wang, Q., Lin, F., He, Q., Liu, X., Xiao, S., Zheng, L., Yang, H., Zhao, H., 2019. Assessment of the
Effects of Bisphenol A on Dopamine Synthesis and Blood Vessels in the Goldfish Brain. Int. J. Mol.
Sci. 20, 6206. https://doi.org/10.3390/ijms20246206

Wetherill, Y.B., Akingbemi, B.T., Kanno, J., McLachlan, J.A., Nadal, A., Sonnenschein, C., Watson,
C.S., Zoeller, R.T., Belcher, S.M., 2007. In vitro molecular mechanisms of bisphenol A action.
Reprod. Toxicol. 24, 178–198. https://doi.org/10.1016/j.reprotox.2007.05.010

Yamada, S., Guo, X., 2018. Peroxiredoxin 4 (PRDX4): Its critical *in vivo* roles in animal models of
metabolic syndrome ranging from atherosclerosis to nonalcoholic fatty liver disease. Pathol. Int.
68, 91–101. https://doi.org/10.1111/pin.12634

Yang, R., Lu, Y., Yin, N., Faiola, F., 2023. Transcriptomic Integration Analyses Uncover Common
Bisphenol A Effects Across Species and Tissues Primarily Mediated by Disruption of JUN/FOS,
EGFR, ER, PPARG, and P53 Pathways. Environ. Sci. Technol. 57, 19156–19168.
https://doi.org/10.1021/acs.est.3c02016

Yazdani, M., Andresen, A.M.S., Gjøen, T., 2016. Short-term effect of bisphenol-a on oxidative stress responses in Atlantic salmon kidney cell line: a transcriptional study. Toxicol. Mech. Methods 26, 295–300. https://doi.org/10.1080/15376516.2016.1177864

Zhang, Y., Han, S., Li, T., Zhu, L., Wei, F., 2024. Bisphenol A induces non-alcoholic fatty liver disease by promoting the O-GlcNAcylation of NLRP3. Arch. Physiol. Biochem. 130, 814–822. https://doi.org/10.1080/13813455.2023.2288533